The development of a method to produce diagnostic reagents using $LaNiO_3$ nanospheres and their application in nanozyme-linked immunosorbent assay

Maria Nikitina*[a,b], Pavel Khramtsov[a,b], Stepan Devyatov[b], Rishat Valeev[c], Marina Eremina[c], Andrey Chukavin[c], and Mikhail Rayev[a,b]

[a] Institute of Ecology and Genetics of Microorganisms, Urals branch of RAS, Perm, Russia.

[b] Biology faculty, Perm State University, Perm, Russia

[c] Udmurt Federal Research Center, Ural Branch of RAS, Izhevsk,Russia.

GRAPHICAL ABSTRACT

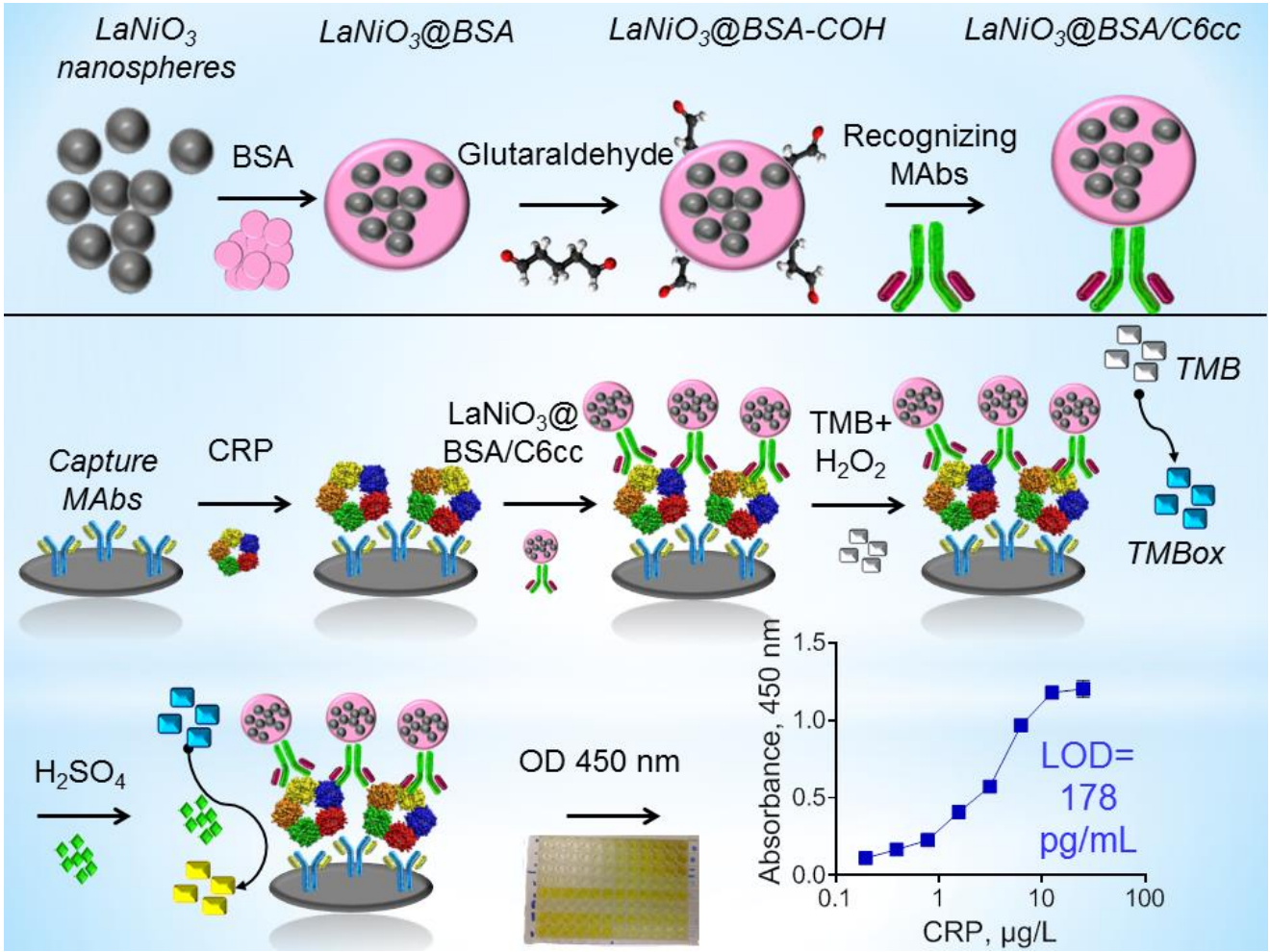

ABSTRACT

Background: LaNiO3 perovskite nanoparticles, especially nanospheres (LNNS), show great promise in biomedical assays due to their peroxidase-like catalytic properties. Methods for synthesizing $LaNiO_3$ nanoparticles of various shapes have been developed, with spherical and rod-shaped $LaNiO_3$ showing better stability. However, LNNS-based diagnostic reagents have not been tested in nanozyme enzyme-linked immunosorbent assay (NLISA) or other enzyme-linked immunosorbent assays, and there is limited data on their synthesis. To fill this gap, it is necessary to develop a method for creating LNNS conjugates with monoclonal antibodies and to investigate the reproducibility, scalability, and applicability of these diagnostic reagents in NLISA.

Results: We have successfully developed a method for producing novel diagnostic reagents utilizing $LaNiO_3$ nanospheres. Our research demonstrates the application of these nanospheres in a NLISA specifically designed for the detection of C-reactive protein (CRP) in real serum samples. This method is both reproducible and scalable, allowing for the efficient production of nanospheres that are functionalized with monoclonal antibodies targeting CRP, with mean diameter of approximately 270 nm. Based on the promising results obtained from our experiments, we have developed and optimized a sandwich-format NLISA for CRP detection. This assay achieved lower limit of detection at 0.178 µg/L, with a dynamic range from 12.5 to 0.195 µg/L and a linear detection range extending from 0.195 to 6.25 µg/L, showcasing its potential for clinical applications.

Significance and Novelty: The new NLISA method, utilizing $LaNiO_3$ nanospheres in a sandwich format for the detection of CRP, significantly enhances sensitivity compared to similar use horseradish peroxidase-based -ELISA. In this study for the first time first the functionalization of lanthanum nickelate nanospheres with recognition elements have demonstrated. This advancement also sheds light on the technological challenges involved in synthesizing diagnostic reagents, identifying areas that need further exploration.

ARTICLE INFO

Keywords
$LaNiO_3$, Nanoparticles,
perovskite, Nanozymes,
Colorimetric immunoassay,
C-reactive protein, NLISA

*Corresponding author.
E-mail addresses:
kropanevamasha@gmail.com
(M. Nikitina)

Highlights

- A novel method for functionalizing LaNiO3 nanospheres has been developed.
- $LaNiO_3$ nanospheres -based NLISA has been demonstrated for the first time.
- The developed NLISA exhibited a LOD of 178 pg/mL.
- A novel NLISA enables the CRP effective detection with high sensitivity.

1. Introduction

Diagnostic tests are the foundation of the healthcare system. The refinement of these techniques still remains a challenge for the scientific community [1]. One of the traditional and widely used methods in laboratory diagnostics is enzyme-linked immunosorbent assay (ELISA). In this type of analysis, the binding of the target marker is quantitatively determined using the colorimetric labels, typically enzyme horseradish peroxidase. However, the application of an enzymatic label as part of a detection reagent presents difficulties. For example, the complexity of the production technology and the high heterogeneity of the resulting enzyme, sensitivity to environmental factors (for example, enzymatic activity decreases in the presence of sodium azide), the dependence on plant-based resources, and insufficient sensitivity for some diagnostic tasks (determination of biomarkers contained in the blood in ultra-low concentrations, for example interleukins [2], [3], [4], [5], [6].

Nanoparticles with peroxidase-like catalytic activity have emerged as a promising alternative to natural enzymes in biosensing and immunoassay applications [7], [8], [9] These nanomaterials can catalyze the oxidation of chromogenic substrates, similar to natural horseradish peroxidase, and be used to amplify signal detection in various bioassays [10].

Perovskite is a ceramic oxide whose molecular formula is ABO_3. The A is usually rare earth metal and the B is transition metal. Both A and B can be replaced by other metal ions of similar radius for forming a variety of compounds. Some studies have shown that perovskite oxide can be used for colorimetric detection by its enzyme-like activity [11,12].

$LaNiO_3$ perovskite nanoparticles have shown promise for use in biomedical assays and immunoassays due to their enzyme-like catalytic properties. It is known that the porous $LaNiO_3$ nanocubes with Ni^{3+} exhibited significantly higher peroxidase-like activity compared to NiO with Ni^{2+} and Ni nanoparticles with Ni^0, about a 58-fold and 22-fold increase, respectively. This enhanced activity was attributed to the 3+ oxidation state of nickel in the $LaNiO_3$ perovskite structure. Leveraging the superior peroxidase-like activity of the porous $LaNiO_3$ nanocubes, the researchers developed facile colorimetric assays for the detection of H_2O_2, glucose, and sarcosine. These assays demonstrated promising applications in clinical diagnostics [13,14]. $LaNiO_3$ perovskite-type oxide nanofibers have been developed into sensors for glucose and hydrogen peroxide [15], as well as a nanozyme-linked immunosorbent assay (NLISA) system for the diagnosis of cancer through the highly sensitive SERS identification of exosomes [16]. Additional confirmation of the high peroxidase-like activity of $LaNiO_3$ perovskite nanoparticles was obtained in 2019 by a group of scientists from China. This study systematically compared more than 20 representative peroxidase-like nanozymes and found that $LaNiO_3$ had the highest peroxidase-like activity [17].

In 2016, Singh and co-author developed methods for preparing cubic, spherical and rod-shaped lanthanum $LaNiO_3$ nanoparticles. Their study also demonstrated the remarkable stability of $LaNiO_3$ nanospheres (LNNS) [18]. However, diagnostic reagents based on LNNS have not yet been tested in NLISA or any other immunoassay, and there is no data on the synthesis of such diagnostic reagents. Therefore, the goal of this work was to optimize the functionalization of spherical $LaNiO_3$ nanoparticles with monoclonal antibodies and study the development process of an NLISA based on them.

As a result, we have developed and optimized a method for producing diagnostic reagents based on LNNS modified with monoclonal antibodies. The functional activity of the resulting diagnostic reagents was demonstrated in a sandwich-format NLISA for the determination of C-reactive protein. The assay parameters, including LOD, dynamic range, linear range, selectivity, accuracy, precision, and inter-day reproducibility, were defined. The convergence of the analysis results with those obtained from a certified clinical diagnostic laboratory was demonstrated. This work also describes, for the first time, the technological difficulties encountered in obtaining diagnostic reagents based on spherical lanthanum nickelate nanoparticles functionalized with monoclonal antibodies.

2. Experemental

The materials and instrumentation utilized in this study are detailed in the Supplementary materials.

2.1. LNNS synthesis

Synthesis of LNNS was conducted as described in [18] with minor modification (Fig. 1, Fig. S1).

In summary, 1.732 g of $La(NO_3)_3 \cdot 6H_2O$ and 1.160 g of $Ni(NO_3)_2 \cdot 6H_2O$ were dissolved in 320 mL of deionized water. The solution was placed in a water bath, and the temperature was raised to 60 °C, matching the solution's temperature. Under continuous stirring at 500 RPM, 80 mL of a 0.375 mol/L NaOH solution was rapidly added, resulting in the formation of a pale green sediment (precursor of nanospheres). The reaction continued for 4 hours, after which the solution was allowed to cool to room temperature. The LNNS precursors settled quickly at the bottom of the glass container, and the excess liquid was discarded. The precipitate was then washed by centrifugation (2000 g for 2 minutes) in 50 mL plastic tubes, repeated five times

with water and once with 95% ethanol. The sediment was transferred to a porcelain cup, dried overnight at 37 °C, and subsequently dried for 5 hours at 70 °C. The dried sample was ground with a pestle and stored at 37 °C for 2 days. Finally, it was calcined at 650 °C for 2 hours, ground again, and stored at room temperature. The final weight of the LNNS powder was 435.4 mg.

2.2. LNNS functionalization by monoclonal antibodies vs CRP

In the first stage, 50 mg of LNNS powder was added to 50 mL of 0.1 mol/L sodium citrate and stirred on a magnetic stirrer at 500 RPM for 3 hours in a water bath maintained at 80 °C (the water bath and reaction medium were kept at the same temperature) (see Fig. 1). The suspension was periodically topped up with water to counteract evaporation. After cooling to room temperature, the mixture was centrifuged at 4000 g for 5 minutes. The sediment was redispersed in 10 mL of water and transferred into 2 mL centrifuge tubes. The nanoparticles were then washed three times with water via centrifugation (10,000 g for 5 minutes). After each wash, the sediment was redispersed by vortexing. Following the final wash, the suspensions were combined, and 1 mol/L sodium citrate was added to achieve a concentration of 1 mmol/L. The resulting suspension was sonicated in an ice bath for 30 minutes using a 3 mm probe at 60% amplification. The final volume of the suspension was 10 mL, with a gravimetric analysis indicating a concentration of 1.4 mg/mL.

Next, BSA (91,5 mg/mL) and LNNS (1.4 mg/mL) were alternately added to 0.05 mol/L HEPES-HCl, pH 7, sonicated (3 mm probe, 60% amplification, 10 s duration), and incubated at +37 °C on a rotator for 60 min. Resulting concentrations of BSA and LNNS were 10 mg/mL and 1 mg/mL, respectively. Obtained solution ($LaNiO_3$@BSA) was dropwise added under vortexing to an equal volume of 25% glutaraldehyde (pH 7, adjusted with 1 mol/L NaOH) and incubated at +37 °C on a rotator for 35 min. The activated $LaNiO_3$@BSA-COH underwent three washes with water through centrifugation at 20000 g for 20 minutes and was subsequently redispersed in 0.05 mol/L HEPES-HCl, pH 7. After each wash $LaNiO_3$@BSA-COH were redispersed by sonication. MAb vs CRP (clone C6cc) was added to $LaNiO_3$@BSA-COH and incubated at +37 °C on a rotator overnight. Resulting concentrations of C6cc was 200 µg/mL.. Then cyanoborohydride to 1mM and glycine to 0.2 M was added for reduction the Schiff bases and blocking unoccupied sites respectively. After 30 min, nanoparticles were washed three times with water. Glycerol up to 20% and BSA up to 1% were added to the resulting diagnostic reagents ($LaNiO_3$@BSA/C6cc) and stored at 4°C.

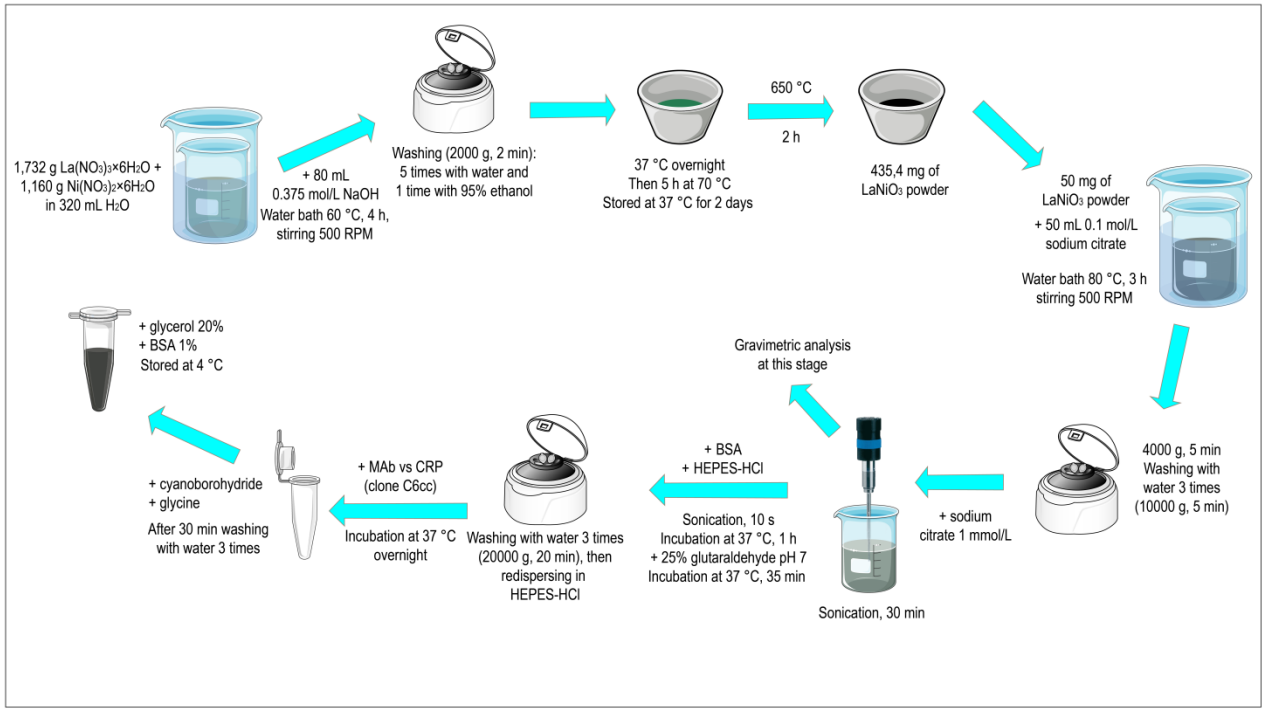

Fig. 1. Scheme of $LaNiO_3$ nanospheres production and modification with Mab

2.3. NLISA of CRP

Capture antibodies (MAbs vs CRP, clone C2) in a carbonate-bicarbonate buffer, pH 9.6 were added into the wells (0.46 μg/mL, 100 μL per well) of a 96-well polystyrene plate and incubated at +4 °C overnight. Then, wells were washed five times with 350 μL PBST using a microplate washer. After that, 250 μL of a blocking solution was added and incubated for 60 min. CRP calibrators diluted in the blocking solution to desired concentrations or analyzed serum samples diluted 1000-fold (100 μL per well) were added, then plates were incubated for 60 min and washed five times. The 100 μL of $LaNiO_3$@BSA/C6cc suspension in the blocking solution was added. After 60 min incubation and washing, 100 μL of the substrate solution was added (Fig. 2). In our previous studies, we conducted a large-scale investigation into how the composition of the substrate buffer affects the analytical signal produced in NLISA using diagnostic reagents based on various nanozymes, including LNNS [19]. The specific composition of the substrate buffer and substrate solution utilized are detailed in the «Materials» section (see Supporting information).

After 20 min (the duration of incubation with the substrate was also determined in the work [19], the reaction was stopped by the addition of 100 μL of 2 M sulphuric acid. The absorbance at 450 nm was measured by a microplate reader. All the assay steps except for the washing and measurement steps were performed in the thermoshaker at +37 °C (mixing speed—350 rpm).

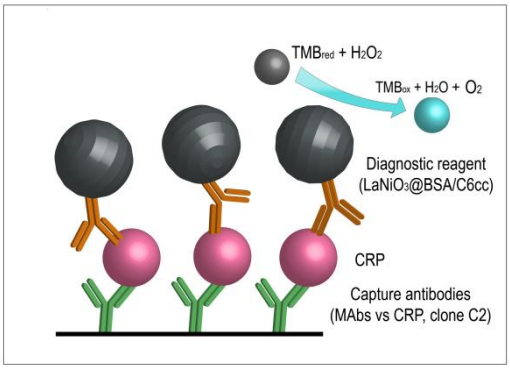

Fig. 2. NLISA for CRP detection based on modified LaNiO3 nanospheres

2.4. Clinical serum samples

Blood serum samples were collected from our laboratory (Laboratory of Cellular Immunology and Nanobiotechnology) as part of various projects investigating post-vaccination immunity in 2022. These serum samples were stored at -20 °C. An immunofluorescence assay was performed on 12 serum samples by the staff of the Department of Faculty Therapy #2, Occupational Pathology, and Clinical Laboratory Diagnostics at Perm State Medical University, named after Academician E. A. Wagner, using certified equipment in accordance with the manufacturer's instructions.

This research was performed according to World Medical Association's Declaration of Helsinki and Council of Europe Protocol to the Convention on Human Rights and Biomedicine and approved by the Ethics Committee of the Institute of Ecology and Genetics of Microorganisms, Ural Branch of the Russian Academy of Sciences (IRB00010009). Written informed consent was obtained from all the participants.

2.5. Data analysis

The acquired data were processed in MS Office Excel, Microsoft (USA). The graphs were prepared in GraphPad Prism 8.01, GraphPad Inc. (USA). The curve fitting was performed in Origin 2019b, OriginLab Corporation (USA).Calibration curve was fitted to a four-parameter logistic model ($1/Y^2$ weighting scheme was used). The general equation of the logistic function was:

$$y = A2 + \frac{A1 - A2}{1 + (\frac{x}{x0})^p}$$

3. Results and discussion

3.1. $LaNiO_3$ nanospheres characterization

The structure of the prepared LNNS was confirmed using several techniques, including X-ray diffraction (Fig.3B, Table 1), UV-Vis spectroscopy, X-ray photoelectron spectroscopy (XPS), and energy-dispersive spectroscopy (EDS) mapping. A detailed analysis of the XPS data can be found in the Supplementary Materials.

XRD analysis of the nanoparticle powder revealed a composition of 73% LaNiO3 phase, with minor contributions from NiO, La_2O_3, and La_2NiO_4. This purity level is lower than the 97% reported by Singh et al. using a similar synthesis method [18]. The reason for this discrepancy remains to be elucidated. Elemental analysis via EDS and XPS confirmed the presence of La, Ni, and O in the LNNS powder (Fig. S2 and S3, and Table S1, S2). Furthermore, the UV-Vis absorbance spectrum of the LNNS aligned with previous reports [19, 20].

Scanning electron microscopy (SEM) revealed that the LNNS exhibited predominantly spherical morphologies with diameters below 50 nm (Fig. 3A). However, this observation contrasts with the mean hydrodynamic diameter determined by dynamic light scattering (DLS) measurements (Z-average: 153-163 nm, with PDI 0.135-0.145), which indicated an average diameter of approximately 160 nm. This discrepancy suggests that the LNNS in colloidal suspension may exist as tightly bound aggregates.

A notable drawback of method for obtaining a LNNS suspension is the significant material loss, which decreased from 50 mg to 14 mg. This loss could affect the scalability of the proposed method for industrial applications.

Table 1
XRD analysis of LNNS;
Rp: 5.88, Rwp: 7.85, Rexp: 3.97, global user-weigthed Chi2=3.92

Phase	Lattice parameter, Å	Weight, %
$LaNiO_3$ (R-3c)	5.4564, 5.4564, 13.1684	73 (72.87)
NiO (Fm-3m)	4.1881	13 (13.21)
La_2O_3 (Ia-3)	11.5274	3 (3.36)
La_2NiO_4 (I4/mmm)	5.2988, 12.9643	10 (10.30)
$LaNiO_3$ (R-3c)	5.4032, 12.4687	0 (0.27)

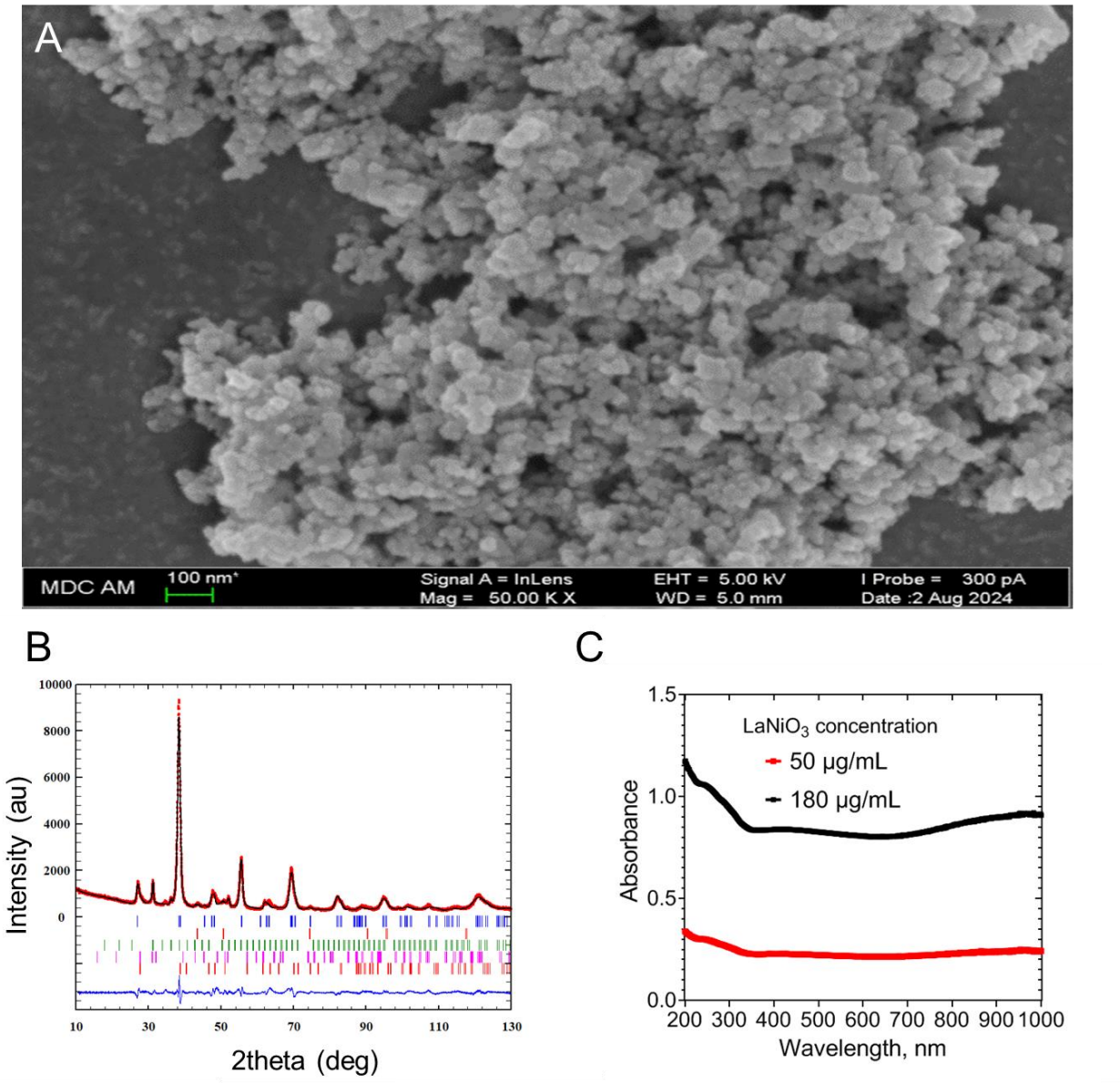

Fig. 3. (A) SEM images of LNNS, scale bars- 100 nm, (B) XRD spectra of LNNS, (C) UV-Vis spectra of LNNS

3.2. Optimization of LNNS conjugates synthesis

It is known that changes in conditions, including composition and molarity of the buffer, can greatly affect the sorption of protein molecules on the surface of nanoparticles [20], [21], [22] In previous studies conducted by our research group, we modified LNNS with recognition elements in a HEPES-HCl buffer [19]. However, the conditions for this modification were not optimized. In the current work, we evaluated how the molarity of the HEPES-HCl buffer affects the results of an immunoassay for the determination of CRP. It has been shown that the employment of a 0.05 M HEPES-HCl buffer for the functionalization of LNNS enables the most sensitive detection of CRP in NLISA (Fig. 4A).

It should be noted that during the stages of BSA sorption, glutaraldehyde activation, and MAb functionalization, the nanospheres aggregated. Stabilization of the LNNS was achieved only at the final stage of producing the diagnostic reagents, after adding up to 1% BSA to the suspension and subjecting it to sonication (Fig. S4). This aggregation complicated the monitoring of the nanospheres concentration using a spectrophotometer at various modification stages. Therefore, for application in NLISA, the absorbance was measured at a wavelength of 450 nm for each diagnostic reagent LaNiO3@BSA/C6cc. In further studies, the concentration of the $LaNiO_3$@BSA/C6cc was expressed as a dilution of 1:100, 1:200, and so on, corrected for differences in optical density.

To antibodies conjugates stabilization, a reaction with sodium cyanoborohydride is used, through which the double bonds of the Schiff bases are reduced [23]. Protocols for reaction using cyanoborohydride exist for conjugates based on horseradish peroxidase [24], as well as for nanoparticles [25] and nanozymes [26]. However, the method of reduction using cyanoborohydride has not been described for LNNS conjugates. Therefore, we tested the effect of the concentration of sodium cyanoborohydride on the functional activity of the $LaNiO_3$@BSA/C6cc (Fig. 4B). It was shown that the addition of $NaBH_3CN$ to a final concentration of 0.0024 and 0.001 mol/L led to the highest functional activity of the LNNS-based diagnostic reagents. The demonstrated decrease in the analytical signal with increasing concentration of the reducing agent cyanoborohydride may be associated with the reduction of Ni^{3+} to Ni^{2+}. It is shown that the high peroxidase-liky activity is associated with the presence of Ni^{3+} in $LaNiO_3$ perovskite-type nanoparticles [13]. For reagent stabilization in further studies, a $NaBH_3CN$ concentration of 0.001 mol/L was used.

In constructing the NLISA, a pair of monoclonal antibodies against CRP (C2-C6cc) was used based on the manufacturer's recommendation. At this stage, the amount of C6cc for $LaNiO_3$@BSA/C6cc modification was optimized. It was shown that the optimal amount of C6cc is 200 µg. It was also demonstrated the absence of non-specific binding of the diagnostic reagent (negative control, BSA on the surface of nanoparticles) with the analysis components (Fig. 4C).

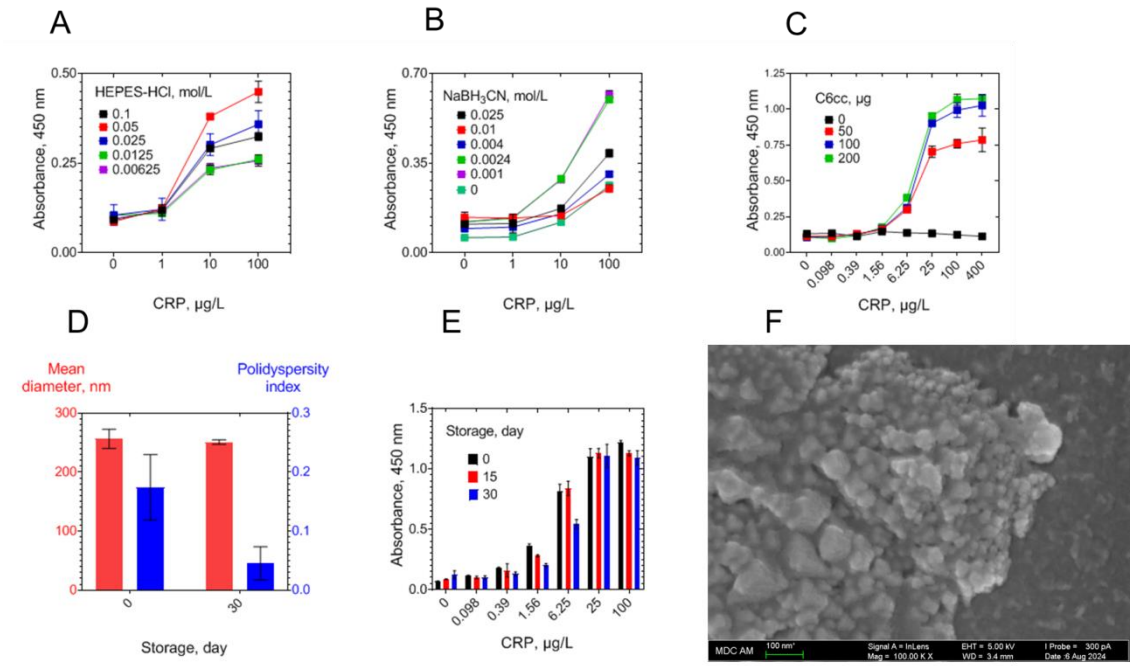

Fig. 4. Results of optimization of the modification process of $LaNiO_3$ nanospheres. (A) Effect of molarity of the coupling buffer; (B) concentration of cyanoborohydride; (C) quantity of monoclonal antibodies on the functional activity of the obtained diagnostic reagents $LaNiO_3$@BSA/C6cc. (D) Evaluation of size and polydispersity; (E) Preservation of colloidal stability during a month of storage at +4C of $LaNiO_3$ nanospheres modified with Mab. Error bars indicate the standard deviation, n = 3; and (F) SEM of the obtained diagnostic reagents $LaNiO_3$@BSA/C6cc. Green line segment is 100 nm.

Figure 4F shows a representative SEM image of the LaNiO3@BSA/C6cc conjugate. The image reveals clusters of nanospheres encapsulated within a protein shell, consistent with the successful functionalization of LNNS. The observed increase in mean hydrodynamic diameter from 160 nm to 270 nm can be attributed to both the presence of the protein layer and potential partial aggregation of LNNS during the functionalization process.

EDS mapping analysis of the LaNiO3@BSA/C6cc conjugate (Fig. S5) further supports the presence of the protein coating. Compared to bare LNNS, the conjugate exhibits an increased carbon content, along with the presence of nitrogen and phosphorus signals. These elements are characteristic components of proteins, confirming the successful protein coating of the LNNS surface. It should be mentioned that the amino acid composition of proteins does not include phosphorus, however, it has been shown that in the process of protein posttranslational modifications this element can appear in their structure [27]. Another explanation for the presence of phosphorus in the LaNiO3@BSA/C6cc suspension may be the adsorption [28] of phosphates on the LNNS surface from monoclonal antibody preparations stored in phosphate-buffered saline [29].

3.3. Storage stability of LNNS-based diagnostic reagents

The change in the sizes and functional activity of diagnostic reagents was studied during storage in H_2O with 1% BSA and 20% glycerol at 4°C. Functional activity was measured by NLISA of CRP. The graphs demonstrate that the dimensions of the $LaNiO_3$@BSA/C6cc remained constant after being stored for 1 month. The polydispersity index, which measures the size distribution, did not exceed 0.2 (Fig. 4D). This indicates that the functionalized LNNS maintained a relatively uniform size during storage

Furthermore, the functional activity of the diagnostic reagent remained stable for 2 weeks of storage. However, after 1 month, a slight decrease in functional activity was observed (Fig. 4E). This decline in the performance of the diagnostic reagent may be attributed to the detachment of antibodies from the surface of the LNNS. This phenomenon could also hinder the integration of LNNS-based diagnostic reagents into actual medical practice. Further experiments are necessary to determine the best storage method, including the composition of the storage buffer and thermal conditions.

3.4. Reproducibility of LNNS-based diagnostic reagent synthesis

While nanozymes hold potential as substitutes for traditional enzymes, additional research is necessary before they can effectively compete in the market. Given that nanozymes are usually created through chemical processes, assessing batch-to-batch consistency is essential. Furthermore, to guarantee that nanozyme-based biosensors and immunoassays can be manufactured on an industrial scale, it is crucial to evaluate the scalability of the production methods for diagnostic reagents derived from them [7], [30].

Therefore, in this work we assessed the reproducibility of the method for obtaining the diagnostic reagent. Also, one of our tasks was to show the scalability of the proposed method for functionalizing LNNS.

On different days, 3 batches of diagnostic reagents were prepared. In this case, two reagents (# 1 and 2) were synthesized in a volume of 500 µl, and the third (# 3) in a volume of 5 ml. After completion of all 3 syntheses, the average size of $LaNiO_3$@BSA/C6cc, its optical density at a wavelength of 450 nm and functional activity were measured. To demonstrate the reproducibility of the method for obtaining diagnostic reagents based on LNNS, CRP was determined in 8 real blood serum samples using 3 batches of diagnostic reagents. Fig. 5 shows the calibration curves and NLISA results for the tree batches. Table 2 demonstrates the concentration, sizes and polydispersity of LNNS and LOD of NLISA.

The concentration, size, and polydispersity of three independent batches of the LNNS diagnostic reagent were nearly identical.

Table 2
Reproducibility of $LaNiO_3$@BSA/C6cc preparation method

Conjugate, №	OD, 450 nm	Mean diameter, nm	LOD, µg/L
1	0.130 ± 0.002	282.4± 2.86	0.42
2	0.133 ± 0.0012	281.3± 8.5	0.53
3	0.138 ± 0.0012	256.7± 13.25	0.33
CV, %	2.47	4.34	19.17

The CRP concentration results for eight serum samples obtained using LNNS-based NLISA across three batches $LaNiO_3$@BSA/C6cc were also consistent (Table S3). The coefficient of variation was from 0.8 to 20.2% (Fig. 5B). In general, the CVs for each sample do not exceed 15%, which is acceptable when developing ELISA [31]. Only the CVs for one sample at a low concentration (0.41 ± 0.08 mg/L) were slightly higher than 20%.

It is important to note that the shapes of the calibration curves and LOD slightly varied. This discrepancy may be attributed to the aggregation of nanoparticles during the surface functionalization process with antibodies, potentially resulting in different levels of antibody adsorption for each batch of the diagnostic reagent (Fig. 5A).

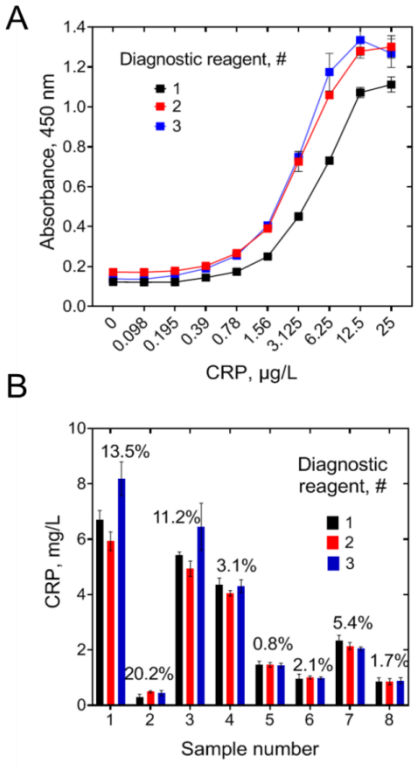

Fig. 5. Reproducibility of $LaNiO_3$@BSA/C6cc preparation method. (A) Calibration curve of NLISA based on 3 batches of $LaNiO_3$@BSA/C6cc diagnostic reagents; (A) CRP level in 8 serum samples determined by NLISA based on 3 batches of $LaNiO_3$@BSA/C6cc diagnostic reagents (CV is indicated at the top of the columns). Error bars indicate the standard deviation, n = 2(A) and n = 5(B)

In a similar study using Prussian blue nanoparticles conjugate for NLISA, slight variations in the limit of detection (scatter of LOD values for Prussian blue nanoparticles-based NLISA: 1.3 – 4.0 ng/mL; CV = 41.6%, n=5) and calibration curve were observed, but the authors deemed the reproducibility of the method for producing diagnostic reagents to be satisfactory [32]. Overall, the results obtained confirm the high reliability of the LNNS-based diagnostic reagents preparation (scatter of LOD values for LNNS-based NLISA: 0.33 –.053 ng/mL, CV = 19.17 %, n=3).

3.5. Optimization of assay

C-reactive protein (CRP) is recognized as a key indicator of inflammation and can also be used to assess the risk of cardiovascular disease [33]. It was found that CRP levels below 1 mg/L indicate a potential risk of cardiovascular disease problems [34]. In the context of the assay design presented in this paper, and considering that serum samples require 1000-fold dilution, we focused on optimizing the assay conditions to generate a calibration curve with a steep slope of approximately 1 µg/L. This strategy will ensure accurate detection of CRP at concentration around 1 µg/L, will making the developed NLISA suitable for assessing cardiovascular risk.

Since the basal level of CRP in blood serum is 1 mg/L [33], finding human blood serum that does not contain CRP is problematic. Commercial mammalian blood sera can be used to optimize the conditions of the NLISA, but there are data on human CRP immunological cross-reactivity with CRP from almost all mammals for which commercially available sera exist (rabbit, bovine, horse, etc.) [35].

We examined the effect of sera from different mammalian species and used a blocking solution as a control. Four different commercial sera were diluted with a blocking solution to 0.1%. CRP was then diluted to 5 µg/L with 0.1% sera and LNNS-based NLISA was performed. It was shown that the use of 0.1% mammalian sera only slightly affects the analytical signal of the developed NLISA (Fig. 6A). In further studies, a blocking solution with the addition of 0.1% rabbit serum was used as a matrix for preparing calibration solutions of CRP (Fig. 6B).

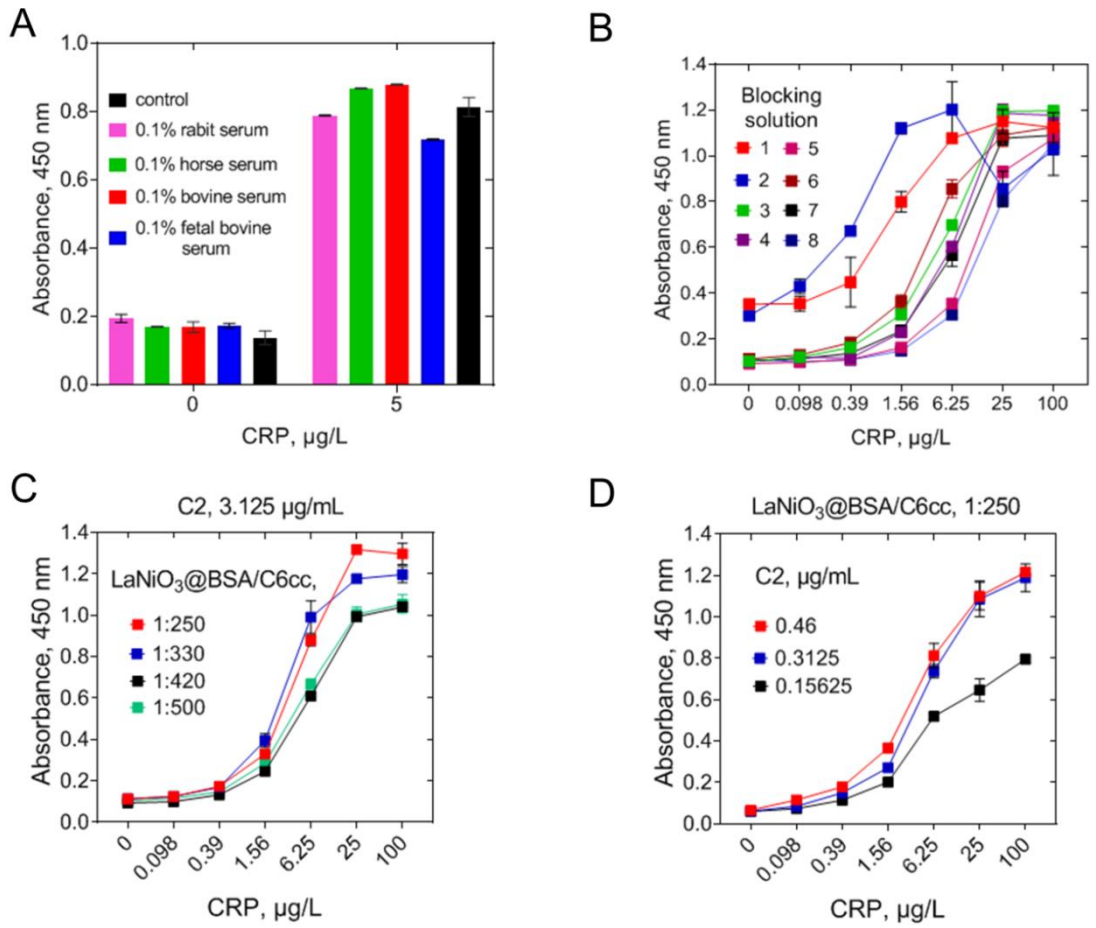

Fig. 6. Evaluation of optimal conditions for NLISA based on $LaNiO_3$@BSA/C6cc. (A) Study of interference with mammalian blood sera. (B) Optimization of the composition of the blocking solution (1.PBST; 2.PBST + 1% BSA; 3.PBST + 0.5% Casein; 4.PBST + 1% Casein; 5.PBST + 2% Casein; 6.PBST + 1% BSA + 0.5% Casein; 7.PBST + 1% BSA + 1% Casein; 8.PBST + 1% BSA + 2% Casein). (C) Optimization of capture monoclonal antibody concentration (D) Optimization of diagnostic reagent dilution; Error bars indicate the standard deviation, n = 3

As part of the optimization of the analysis procedure, the following parameters were optimized:

1) Concentration of the first (capturing) monoclonal antibodies (clone C2);
2) Dilution of the diagnostic reagent $LaNiO_3$@BSA/C6cc;
3) Composition of the blocking buffer.

The optimization results are presented in Fig. 6 B, C and D. It has been shown that the optimal parameters are:

1) Concentration of C2: 0.46 μg/ml;
2) $LaNiO_3$@BSA/C6cc dilution: 1:250;
3) The optimal blocking effect is achieved when using PBST with 1% BSA and 0.5% Casein as a blocking buffer.

3.6. Analytical performance of LNNS-based NLISA

Experiments, dedicated to analytical performance of NLISA were conducted under optimal assay parameters.

3.6.1. NLISA selectivity

Selectivity was determined using three human inflammatory markers: procalcitonin [36], serum amyloid A1 and A2 (SAA1 and SAA2) [37]; and canine CRP (CRPc). Also the selectivity of the assay was confirmed using a protein from the pentraxin family: human serum amyloid P component (SAP) [38]. SAP gene, recognized as a close paralog of CRP, is also situated on chromosome 1q23.2 and exhibits a similar gene structure, potentially causing nonspecific binding and compromising the precision of the assay under development [39], [40]. The analyzed markers were diluted to the required concentrations 5 and 50 μg /mL with a blocking solution with 0.1% rabbit serum. The studied markers concentrations were selected based on their basal levels in the blood. There was no detectable analytical signal in samples containing 5 and 50 μg /mL PCT, SAA1, SAA2, SAP or CRPc (Fig. 7D).

In the subsequent experiments, we assessed following analytical parameters of the assay, including the limit of detection (LOD), upper limit of quantification (ULOQ), lower limit of quantification (LLOQ), linear range, accuracy, precision, inter-day reproducibility and conducted a comparison with a reference CRP immunoassay. The calibration plot was constructed under optimal experimental conditions using rabbit serum diluted 1000-fold as a matrix. The four-parameter и

3.6.2. LLOQ, ULOQ, linear range and LOD of LNNS-based NLISA

In validation experiments 10 calibrators were used (0 to 25 μg/L CRP) (Fig. 7A). Every calibrator was tested in 10 replicates . The LOD (blank + 3 × SD) was 0.178 μg/L (178 pg/mL) (Fig 7A).

For the assessment of the ULOQ and LLOQ, a spike-recovery test and coefficient of variation (CV) calculation were conducted. Rabbit serum was diluted 1000-fold and spiked with C-reactive protein (CRP) at ten different concentrations, each tested in eight replicates (Table S4). The CRP concentrations in the spiked samples were determined using a calibration curve, and the CV was calculated for each sample. The CV ranged from 2.59% to 55%. The method developed allows for the determination of CRP with a CV of less than 25% within a concentration range of 0.195 to 12.5 μg/L (Table S2). The recovery index also met acceptable criteria for ULOQ and LLOQ (75% to 125%) for CRP concentrations between 0.195 and 12.5 μg/L, (TableS4) [41], [42]. Therefore, the ULOQ and LLOQ for the NLISA for CRP detection using LNNS are 12.5 μg/L and 0.195 μg/L, respectively (Fig. 7C). The developed analysis allows to determine CRP in blood serum with a linear range of 0.195-6.25 μg/L respectively (r^2 = 0.988) (Fig. 7D).

3.6.3. NLISA accuracy

The spike-recovery test was performed for five CRP concentrations to assess the accuracy of the developed NLISA. Since blood serum samples are planned to be diluted 1000 times, this experiment simulated a situation where a CRP sample was diluted 1000 times. CRP at concentrations of 13, 5, 1, 0.6, and 0.35 mg/L was added to whole rabbit blood serum in 6 replicates. The resulting samples were diluted 1/1000 with a blocking solution, and CRP was determined using the developed method. A calibration curve was constructed for 10 points in triplicates (from 0 to 25 μg/L). The obtained concentrations were multiplied by the dilution factor and expressed in mg/L. The recovery index varied from 76 to 102.9% (Table S5), CV didn't overshoot 15%. These results correlate with the results of the lower limit of quantification (LLOQ), upper limit of

quantification (ULOQ), and linear range assessment, indicating that diluting samples by a factor of 1000 has no impact on the analytical performance of the assay.

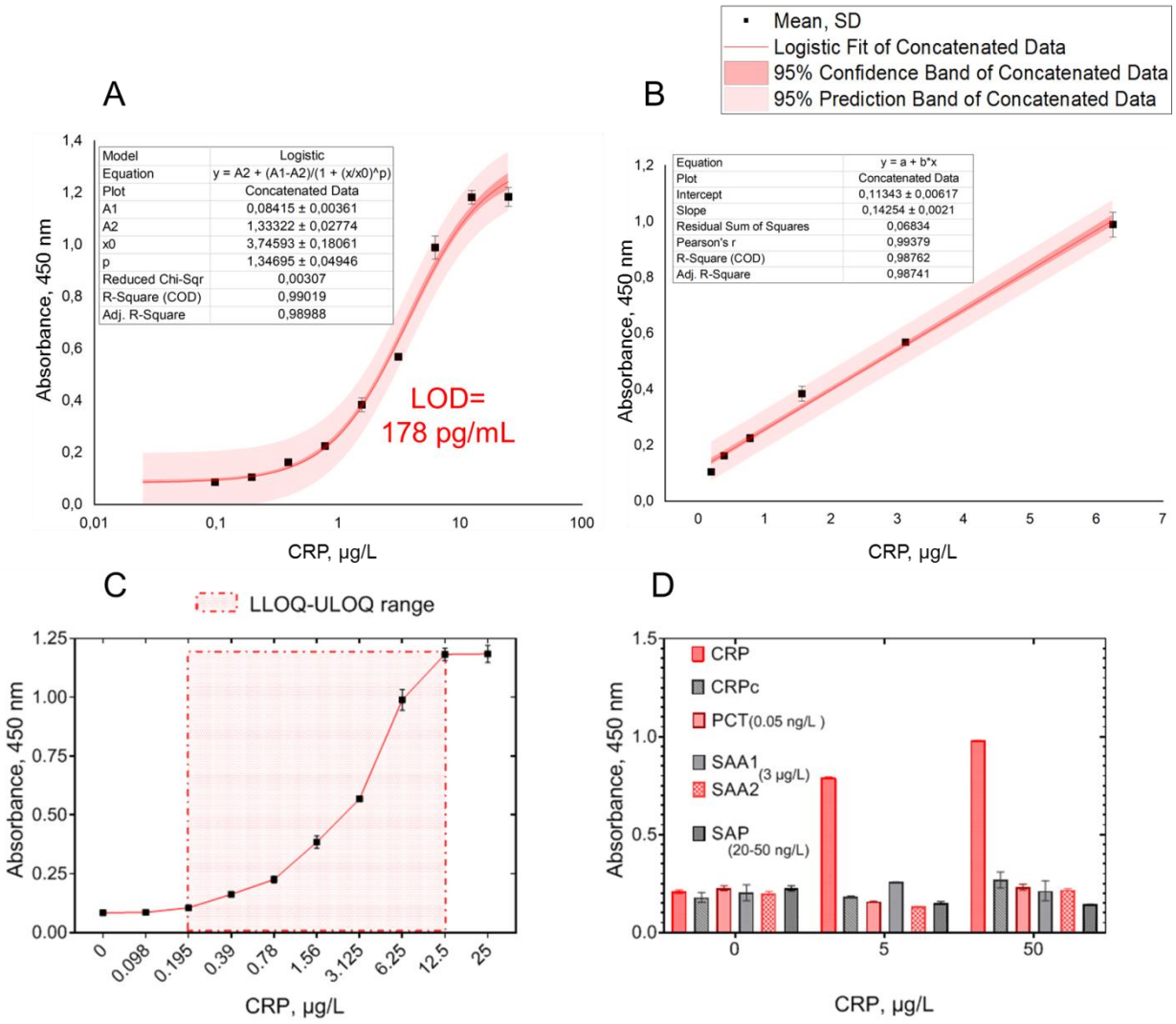

Fig. 7. Performance of the developed NLISA. (A) Calibration curve and LOD; (B) Linear range; (C) ULOQ/LLOQ range; (D) Selectivity of assay (The basal level of the marker is indicated in brackets, taking into account the 1000-dilution of the serum blood samples). Error bars indicate the standard deviation, n = 10 (A, B, C) and n = 3 (D)

3.6.4. NLISA precision and inter-day reproducibility

To evaluate the precision, 8 real samples in 8 replicates were tested by the proposed method (Table S6). For each serum, the CV did not exceed 20% which corresponds to the approved level [41], [43].

As part of the validation process for the developed immunoassay, studies were conducted to evaluate the inter-day reproducibility of the assay results. To achieve this, NLISA was performed over five days to measure CRP levels in ten blood serum samples (n=3). Each day, new plates with immobilized MAbs (clone C2) were prepared, along with fresh wash, blocking, and substrate buffers. Calibration curves were created using ten points (ranging from 0 to 25 µg/L) (Fig. 8). The average value from the three replicates was calculated for each of the ten blood serum samples (Table 2). Subsequently, the CV was computed for each sample (n=5) (Table S7).

The results indicated that the calibration curves for CRP determination using the NLISA method with LNNS, obtained from five separate analyses, were nearly identical (Fig. 8). Table 3 demonstrates that the coefficient of variation does not exceed 20% for all ten blood serum samples.

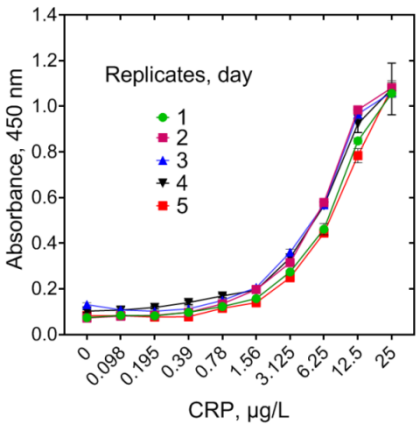

Fig. 8. Calibration curves obtained on different days. Error bars indicate the standard deviation, n = 2

Table 3
Inter-day reproducibility of LNNS-based NLISA

Sample number	Mean (n=5), mg/L	SD	CV,%
1	1.1	0.22	19.6
2	14.11	1.26	8.92
3	1.02	0.17	16.76
4	10.72	0.98	9.16
5	9.09	1.24	13.60
6	2.75	0.18	6.63
7	15.66	1.47	9.40
8	2.02	0.18	9.03
9	4.15	0.28	6.76
10	2.36	0.47	19.88

3.6.5. Comparison of NLISA with reference method

We assessed the concentration of C-reactive protein (CRP) in 12 blood serum samples collected from volunteers using NLISA with three replicates. Calibration curves were established with ten points, ranging from 25 to 0 µg/ml. CRP levels in these samples were measured using an immunofluorescence assay at a certified clinical laboratory. The comparison of results is illustrated in Fig. 9. as a Bland-Altman plot. The Bland-Altman analysis revealed no significant bias between the two methods, with the immunofluorescence assay yielding an average CRP concentration that was only 4.5 % higher (bias: -4.486 %, 95% CI from -31.26 to 22.29%).

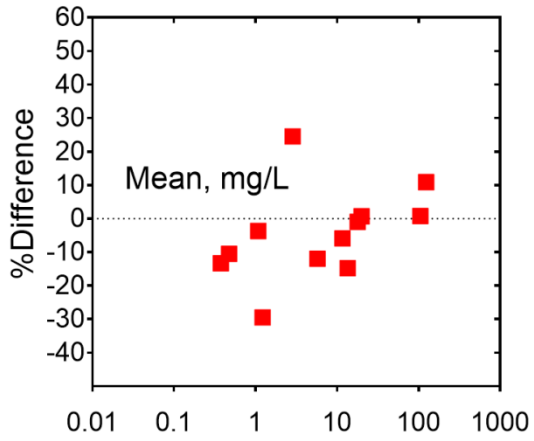

Fig. 9. Bland-Altman plot comparing NLISA based on $LaNiO_3$ nanospheres and immunofluorescence assay. X axis—mean of CRP concentrations measured by two methods. Y axis—the difference between concentrations measured by two methods divided by the average concentration measuredby both methods (in percent).

Variations in results between the two laboratories may be attributed to differences in equipment and reagents. Furthermore, samples from the clinical laboratory were stored at -20 °C for six months, during which the conformation of CRP may have altered, potentially affecting its binding ability to the capturing (C2) and recognizing (clone C6cc) monoclonal antibodies. It is also important to note that the analyses were conducted by different operators.

In conclusion, the data presented indicates that the results obtained from different methods in two independent laboratories are comparable. The level of differences according to Bland-Altman analysis does not exceed 30% (Table S8).

4. Conclusions

In this study, we present a novel method for producing diagnostic reagents using $LaNiO_3$ nanospheres and their application in a NLISA. CRP was selected as the target analyte. The synthesis of the LNNS conjugate with monoclonal antibodies against CRP was optimized. Reproducibility and scalability of the production method were confirmed. Also, the colloidal stability of the obtained conjugates during 1 month of storage was demonstrated. Using the obtained conjugates, a sandwich-format NLISA was designed and optimized. The assay demonstrated a detection limit of 0.178 µg/L with a linear range from 0.195 to 6.25 µg/L. Based on these data and validation experiments, the developed assay can be used for primary prevention of cardiovascular diseases, categorizing relative risk levels as low (<1.0 mg/L), intermediate (1.0–3.0 mg/L), and high (>3.0 mg/L) according to CDC/AHA guidelines [33], [34].

The NLISA method utilizing $LaNiO_3$ nanospheres is comparable to highly sensitive immunoassays and immunosensors developed in the past year (Table 4). A comparison was also conducted with two commercial ELISA kits based on existing literature [44], [45]. Results indicated that the lower limit of detection for the ELISA in a sandwich format (without the biotin enhancement step) is significantly higher than that of the NLISA in the same format presented in this study (50 ng/ml compared to 0.178 ng/ml).

Moreover, the functionalization process of lanthanum nickelate nanospheres with recognition molecules has been demonstrated for the first time. It provides new insights into the technological challenges associated with diagnostic reagent production, highlighting areas that require further investigation:

- low yield of nanospheres when obtaining a suspension;
- aggregation of nanospheres when functionalized with antibodies;
- decrease in functional activity during storage.

Table 4

The comparison of performance of different CRP assays

Method	Linear range	LOD	Ref.
Carbon nanotube field-effect transistor (CNT-FET) immunosensor	0.01–1000 μg/mL	0.06 μg/mL	[46]
Label-free electrochemical aptasensor based on Ti3C2Tx-Ag/Au nanoparticles	0.1–200 ng/mL	41 pg/mL	[47]
Label-free electrochemical detection of C-reactive protein on a peptide receptor−gold nanoparticle−black phosphorous nanocomposite modified electrode	0–0.036 μg/mL	0.7 ng/mL.	[48]
One-step paper-based SlipChip for the sensitive detection of C-reactive protein with porous platinum nanozyme-assisted signal amplification	0.1-1000 ng/mL	30 pg/mL	[49]
Commercial ELISA without biotin enhancement	0.25–25 μg/mL	50 ng/mL	[44]
Commercial ELISA with biotin enhancement	18.75–1600 pg/mL	< 10 pg/mL	[45]
NLISA with Prussian blue nanozyme	0.39–50 ng/mL	21.8 pg/mL	[50]
NLISA with LaNiO3 nanospheres	0.195–12.5 ng/mL	178 pg/mL	This work

In summary, we would like to emphasize that perovskite-type nanospheres of lanthanum nickelate have potential as diagnostic reagents for colorimetric immunoassays. However, the current method for producing unprocessed nanospheres is both time-consuming and labor-intensive, and resulting in a very low yield of LNNS suitable for further MAbs functionalization. This limitation may impact the practical application of the proposed nanospheres.

In this work, we presented the results of the development of NLISA for the detection of CRP. This marker is contained in the blood in fairly high concentrations. Therefore, it is premature to conclude that the developed LNNS-based NLISA will be effective for detecting markers in ultra-low concentrations.

Supplementary information

The online version contains supplementary material

CRediT authorship contribution statement

Maria Nikitina: Conceptualization, Investigation, Project administration, Validation, Visualization, Writing – original draft, Writing – review & editing. **Pavel Khramtsov**: Conceptualization, Supervision, Writing – original draft, Writing – review & editing. **Stepan Devyatov**: Investigation, Writing – original draft. **Rishat Valeev**– Investigation, Writing – original draft. **Marina Eremina**: Investigation, Writing – original draft. **Andrey Chukavin**: Investigation, Writing – original draft. **Mikhail Rayev**: Conceptualization, Resources, Validation, Writing – review & editing.

Declaration of competing interest

The authors declare that they have no known competing financial interests or personal relationships that could have appeared to influence the work reported in this paper.

Data availability

No data was used for the research described in the article

Acknowledgements

This study was carried out within the framework of the State assignment of Ministry of Science and Higher Education of the Russian Federation (registration number # 124020500027-7).

SEM images, XRD pattern and XPS spectra were recorded on the equipment of Center of Collective Use “Center of physical and physical-chemical methods of analysis, investigations of properties and characteristics of surface, nanostructures, materials and products” of Udmurt Federal Research Center of UB RAS. Modernization of Specs XPS spectrometer was supported by Russian Ministry of Science and Education (agreement # 075-15-2021-1351).

The authors express their gratitude to Dmitry Yuryevich Sosnin, professor of the Department of Faculty Therapy #2, Occupational Pathology and Clinical Laboratory of Diagnostics Perm State Medical University named after Academician E. A. Wagner, for his valuable assistance in conducting the immunofluorescent assay.

References

[1] R.W. Peeling, D.L. Heymann, Y.-Y. Teo, P.J. Garcia, Diagnostics for COVID-19: moving from pandemic response to control, The Lancet 399 (2022) 757–768. https://doi.org/10.1016/S0140-6736(21)02346-1.

[2] Y. Luo, M. Pehrsson, L. Langholm, M. Karsdal, A.-C. Bay-Jensen, S. Sun, Lot-to-Lot Variance in Immunoassays—Causes, Consequences, and Solutions, Diagnostics 13 (2023) 1835. https://doi.org/10.3390/diagnostics13111835.

[3] F.W. Krainer, M.A. Gerstmann, B. Darnhofer, R. Birner-Gruenberger, A. Glieder, Biotechnological advances towards an enhanced peroxidase production in Pichia pastoris, J. Biotechnol. 233 (2016) 181–189. https://doi.org/10.1016/j.jbiotec.2016.07.012.

[4] Z. Almaz, A. Oztekin, N. Abul, S. Gerni, D. Erel, S.M. Kocak, M.E. Sengül, H. Ozdemir, A new approach for affinity-based purification of horseradish peroxidase, Biotechnol. Appl. Biochem. 68 (2021) 102–113. https://doi.org/10.1002/bab.1899.

[5] P. Peng, C. Liu, Z. Li, Z. Xue, P. Mao, J. Hu, F. Xu, C. Yao, M. You, Emerging ELISA derived technologies for in vitro diagnostics, TrAC Trends Anal. Chem. 152 (2022) 116605. https://doi.org/10.1016/j.trac.2022.116605.

[6] S. Hosseini, P. Vázquez-Villegas, M. Rito-Palomares, S.O. Martinez-Chapa, Advantages, Disadvantages and Modifications of Conventional ELISA, in: Enzyme-Linked Immunosorbent Assay ELISA, Springer Singapore, Singapore, 2018: pp. 67–115. https://doi.org/10.1007/978-981-10-6766-2_5.

[7] C.P. Kurup, M.U. Ahmed, Nanozymes towards Personalized Diagnostics: A Recent Progress in Biosensing, Biosensors 13 (2023) 461. https://doi.org/10.3390/bios13040461.

[8] H.A. Elkomy, S.A. El-Naggar, M.A. Elantary, S.M. Gamea, M.A. Ragab, O.M. Basyouni, M.S. Mouhamed, F.F. Elnajjar, Nanozyme as detector and remediator to environmental pollutants: between current situation and future prospective, Environ. Sci. Pollut. Res. 31 (2023) 3435–3465. https://doi.org/10.1007/s11356-023-31429-0.

[9] L. Zhou, Y. Liu, Y. Lu, P. Zhou, L. Lu, H. Lv, X. Hai, Recent Advances in the Immunoassays Based on Nanozymes, Biosensors 12 (2022) 1119. https://doi.org/10.3390/bios12121119.

[10] E.M. Hamed, V. Rai, S.F.Y. Li, Single-atom nanozymes with peroxidase-like activity: A review, Chemosphere 346 (2024) 140557. https://doi.org/10.1016/j.chemosphere.2023.140557.

[11] L. Song, Y. Zhu, Z. Yang, C. Wang, X. Lu, Oxidase-mimicking activity of perovskite $LaMnO_{3+\delta}$ nanofibers and their application for colorimetric sensing, J. Mater. Chem. B 6 (2018) 5931–5939. https://doi.org/10.1039/C8TB01706A.

[12] K. Wang, J. Song, X. Duan, J. Mu, Y. Wang, Perovskite $LaCoO_3$ nanoparticles as enzyme mimetics: their catalytic properties, mechanism and application in dopamine biosensing, New J. Chem. 41 (2017) 8554–8560. https://doi.org/10.1039/C7NJ01177F.

[13] X. Wang, W. Cao, L. Qin, T. Lin, W. Chen, S. Lin, J. Yao, X. Zhao, M. Zhou, C. Hang, H. Wei, Boosting the Peroxidase-Like Activity of Nanostructured Nickel by Inducing Its 3+ Oxidation State in $LaNiO_3$ Perovskite and Its Application for Biomedical Assays, Theranostics 7 (2017) 2277–2286. https://doi.org/10.7150/thno.19257.

[14] N. Xu, S. Jin, L. Wang, Metal nanoparticles-based nanoplatforms for colorimetric sensing: A review, Rev. Anal. Chem. 40 (2020) 1–11. https://doi.org/10.1515/revac-2021-0122.

[15] B. Wang, S. Gu, Y. Ding, Y. Chu, Z. Zhang, X. Ba, Q. Zhang, X. Li, A novel route to prepare $LaNiO_3$ perovskite-type oxide nanofibers by electrospinning for glucose and hydrogen peroxide sensing, The Analyst 138 (2013) 362–367. https://doi.org/10.1039/C2AN35989H.

[16] Q. Zhao, H. Wang, W. Jiang, H. Gao, S. Wen, X. Feng, Q. Wu, C. He, Y. Zhu, L. Hu, B. Zhao, W. Song, SERS Resolving of the Significance of Acetate on the Enhanced Catalytic Activity of Nanozymes, Anal. Chem. 94 (2022) 17930–17938. https://doi.org/10.1021/acs.analchem.2c03992.

[17] X. Wang, X.J. Gao, L. Qin, C. Wang, L. Song, Y.-N. Zhou, G. Zhu, W. Cao, S. Lin, L. Zhou, K. Wang, H. Zhang, Z. Jin, P. Wang, X. Gao, H. Wei, eg occupancy as an effective descriptor for the catalytic activity of perovskite oxide-based peroxidase mimics, Nat. Commun. 10 (2019) 704. https://doi.org/10.1038/s41467-019-08657-5.

[18] S. Singh, D. Zubenko, B.A. Rosen, Influence of $LaNiO_3$ Shape on Its Solid-Phase Crystallization into Coke-Free Reforming Catalysts, ACS Catal. 6 (2016) 4199–4205. https://doi.org/10.1021/acscatal.6b00673.

[19] P. Khramtsov, R. Valeev, M. Eremina, M. Rayev, Enhancing Nanozyme-Based Colorimetric Assays by Optimizing Substrate Composition, (2024). https://doi.org/10.26434/chemrxiv-2024-prpb7.

[20] R. Eigenheer, E.R. Castellanos, M.Y. Nakamoto, K.T. Gerner, A.M. Lampe, K.E. Wheeler, Silver nanoparticle protein corona composition compared across engineered particle properties and environmentally relevant reaction conditions, Env. Sci Nano 1 (2014) 238–247. https://doi.org/10.1039/C4EN00002A.

[21] B. Jachimska, A. Pajor, Physico-chemical characterization of bovine serum albumin in solution and as deposited on surfaces, Bioelectrochemistry 87 (2012) 138–146. https://doi.org/10.1016/j.bioelechem.2011.09.004.

[22] O. Moradi, M.S. Maleki, S. Tahmasebi, Comparison between Kinetics Studies of Protein Adsorption by Single-walled Carbon Nanotube and Gold Nanoparticles Surfaces, Fuller. Nanotub. Carbon Nanostructures 21 (2013) 733–748. https://doi.org/10.1080/1536383X.2012.654536.

[23] I. Migneault, C. Dartiguenave, M.J. Bertrand, K.C. Waldron, Glutaraldehyde: Behavior in Aqueous Solution, Reaction with Proteins, and Application to Enzyme Crosslinking, BioTechniques 37 (2004) 790–802. https://doi.org/10.2144/04375RV01.

[24] V.C.W. Tsang, R.M. Greene, J.B. Pilcher, Optimization of the Covalent Conjugating Procedure ($NaIO_4$) of Horseradish Peroxidase to Antibodies for Use in Enzyme-Linked Immunosorbent Assay, J. Immunoassay 16 (1995) 395–418. https://doi.org/10.1080/15321819508013570.

[25] R.G. DiScipio, Preparation of Colloidal Gold Particles of Various Sizes Using Sodium Borohydride and Sodium Cyanoborohydride, Anal. Biochem. 236 (1996) 168–170. https://doi.org/10.1006/abio.1996.0146.

[26] X. Li, G. Lin, L. Zhou, O. Prosser, M.H. Malakooti, M. Zhang, Green synthesis of iron-doped graphene quantum dots: an efficient nanozyme for glucose sensing, Nanoscale Horiz. 9 (2024) 976–989. https://doi.org/10.1039/D4NH00024B.

[27] S. Ramazi, J. Zahiri, Post-translational modifications in proteins: resources, tools and prediction methods, Database 2021 (2021) baab012. https://doi.org/10.1093/database/baab012.

[28] M. Li, M. Feng, C. Guo, S. Qiu, L. Zhang, D. Zhao, H. Guo, K. Zhang, F. Wang, Green and Efficient Al-Doped $LaFe_xAl_{1-x}O_3$ Perovskite Oxide for Enhanced Phosphate Adsorption with Creation of Oxygen Vacancies, ACS Appl. Mater. Interfaces 15 (2023) 16942–16952. https://doi.org/10.1021/acsami.2c19513.

[29] Моноклональные антитела к С-реактивному белку (CRP) - купить недорого, цены в компании Хайтест, (n.d.). https://products.hytest.ru/product/c-reactive-protein-crp-antibody (accessed August 12, 2024).

[30] Z. Farka, J.C. Brandmeier, M.J. Mickert, M. Pastucha, K. Lacina, P. Skládal, T. Soukka, H.H. Gorris, Nanoparticle-Based Bioaffinity Assays: From the Research Laboratory to the Market, Adv. Mater. 36 (2024) 2307653. https://doi.org/10.1002/adma.202307653.

[31] J.R. Crowther, The ELISA Guidebook, Humana Press, Totowa, NJ, 2009. https://doi.org/10.1007/978-1-60327-254-4.

[32] Z. Farka, V. Čunderlová, V. Horáčková, M. Pastucha, Z. Mikušová, A. Hlaváček, P. Skládal, Prussian Blue Nanoparticles as a Catalytic Label in a Sandwich Nanozyme-Linked Immunosorbent Assay, Anal. Chem. 90 (2018) 2348–2354. https://doi.org/10.1021/acs.analchem.7b04883.

[33] I. Kushner, C-reactive protein – My perspective on its first half century, 1930-1982, Front. Immunol. 14 (2023) 1150103. https://doi.org/10.3389/fimmu.2023.1150103.

[34] T.A. Pearson, G.A. Mensah, R.W. Alexander, J.L. Anderson, R.O. Cannon, M. Criqui, Y.Y. Fadl, S.P. Fortmann, Y. Hong, G.L. Myers, N. Rifai, S.C. Smith, K. Taubert, R.P. Tracy, F. Vinicor, Markers of Inflammation and Cardiovascular Disease: Application to Clinical and Public Health Practice: A Statement for Healthcare Professionals From the Centers for Disease Control and Prevention and the American Heart Association, Circulation 107 (2003) 499–511. https://doi.org/10.1161/01.CIR.0000052939.59093.45.

[35] A. Pathak, A. Agrawal, Evolution of C-Reactive Protein, Front. Immunol. 10 (2019) 943. https://doi.org/10.3389/fimmu.2019.00943.

[36] I. Samsudin, S.D. Vasikaran, Clinical Utility and Measurement of Procalcitonin, Clin. Biochem. Rev. 38 (2017) 59–68.

[37] I. Sorić Hosman, I. Kos, L. Lamot, Serum Amyloid A in Inflammatory Rheumatic Diseases: A Compendious Review of a Renowned Biomarker, Front. Immunol. 11 (2021) 631299. https://doi.org/10.3389/fimmu.2020.631299.

[38] D. Pilling, R.H. Gomer, The Development of Serum Amyloid P as a Possible Therapeutic, Front. Immunol. 9 (2018) 2328. https://doi.org/10.3389/fimmu.2018.02328.

[39] Z. Wang, X. Wang, H. Zou, Z. Dai, S. Feng, M. Zhang, G. Xiao, Z. Liu, Q. Cheng, The Basic Characteristics of the Pentraxin Family and Their Functions in Tumor Progression, Front. Immunol. 11 (2020) 1757. https://doi.org/10.3389/fimmu.2020.01757.

[40] D. Xi, T. Luo, H. Xiong, J. Liu, H. Lu, M. Li, Y. Hou, Z. Guo, SAP: structure, function, and its roles in immune-related diseases, Int. J. Cardiol. 187 (2015) 20–26. https://doi.org/10.1016/j.ijcard.2015.03.179.

[41] Bioanalytical Method Validation Guidance for Industry, (2018).

[42] An Explanation of Sensitivity and the LLD, LLOQ, and ULOQ of a Multiplex ELISA, (2020). https://www.quansysbio.com/support/explanation-of-sensitivity-lld-lloq-and-uloq/ (accessed August 2, 2024).

[43] M. Azadeh, P. Sondag, Y. Wang, M. Raines, J. Sailstad, Quality Controls in Ligand Binding Assays: Recommendations and Best Practices for Preparation, Qualification, Maintenance of Lot to Lot Consistency, and Prevention of Assay Drift, AAPS J. 21 (2019) 89. https://doi.org/10.1208/s12248-019-0354-6.

[44] С-реактивный белок СРБ ИФА - купить в Екатеринбурге, (n.d.). https://art-medika.com/catalog/IFA/aytoimmyn/product-5761.html (accessed August 5, 2024).

[45] MAN0004010_KHA0031_HuCRP_ELISA_PI.pdf, (n.d.). https://assets.thermofisher.com/TFS-Assets/LSG/manuals/MAN0004010_KHA0031_HuCRP_ELISA_PI.pdf (accessed August 5, 2024).

[46] G. Rabbani, M.E. Khan, E. Ahmad, M.V. Khan, A. Ahmad, A.U. Khan, W. Ali, M.A. Zamzami, A.H. Bashiri, W. Zakri, Serum CRP biomarker detection by using carbon nanotube field-effect transistor (CNT-FET) immunosensor, Bioelectrochemistry 153 (2023) 108493. https://doi.org/10.1016/j.bioelechem.2023.108493.

[47] K. Li, Z. Shi, Y. Wang, F. Yan, Z. Li, Z. Wang, Z. Zhu, A label-free electrochemical aptasensor based on Ti3C2Tx-Ag/Au nanoparticles as a signal amplification strategy for CRP detection, Microchem. J. 195 (2023) 109479. https://doi.org/10.1016/j.microc.2023.109479.

[48] H.J. Yang, M.W. Kim, C.V. Raju, C.H. Cho, T.J. Park, J.P. Park, Highly sensitive and label-free electrochemical detection of C-reactive protein on a peptide receptor−gold nanoparticle−black phosphorous nanocomposite modified electrode, Biosens. Bioelectron. 234 (2023) 115382. https://doi.org/10.1016/j.bios.2023.115382.

[49] S.E. Son, S.H. Cheon, W. Hur, H.B. Lee, D.H. Kim, C.H. Ha, S.J. Lee, D.K. Han, G.H. Seong, One-step paper-based SlipChip for the sensitive detection of C-reactive protein with porous platinum nanozyme-assisted signal amplification, Biosens. Bioelectron. 243 (2024) 115752. https://doi.org/10.1016/j.bios.2023.115752.

[50] M. Nikitina, P. Khramtsov, M. Bochkova, M. Rayev, Development and performance of NLISA for C-reactive protein detection based on Prussian blue nanoparticle conjugates, Anal. Bioanal. Chem. 416 (2024) 3097–3106. https://doi.org/10.1007/s00216-024-05268-y.

Supplementary materials

The development of a method to produce diagnostic reagents using $LaNiO_3$ nanospheres and their application in nanozyme-linked immunosorbent assay

Maria Nikitina*[a,b], Pavel Khramtsov[a,b], Stepan Devyatov[b], Rishat Valeev[c], Marina Eremina,[c], Andrey Chukavin,[c] and Mikhail Rayev[a,b]

[a] Institute of Ecology and Genetics of Microorganisms, Urals branch of RAS, Perm, Russia.

[b] Biology faculty, Perm State University, Perm, Russia

[c] Udmurt Federal Research Center, Ural Branch of RAS, Izhevsk, Russia.

ARTICLE INFO

Keywords
$LaNiO_3$, Nanoparticles,
pervoskite, Nanozymes,
Colorimetric immunoassay,
C-reactive protein, ELISA

*Corresponding author.
E-mail addresses:
kropanevamasha@gmail.com
(M. Nikitina)

Materials

Tween-20, glutaraldehyde, citric acid, glycine, sodium phosphate, sodium bicarbonate, and glycerol were from ITW (USA). Citric acid and MES was from Helicon (Russia). Mouse monoclonal IgG2a against human CRP (clone C2 and C6cc) further designated as C2 and C6cc, recombinant human CRP, procalcitonin (PCT), Serum amyloid A1 and A2 (SAA1 and SAA2), and canine CRP (CRPc) were obtained from HyTest (Finland). Human serum amyloid P component (SAP) was from CusaBio (China). Casein, 11.77 M hydrogen peroxide were from Sigma-Aldrich (USA). Bovine serum albumin was from Biosera (France). 3,3',5,5'-tetramethylbenzidine dihydrochloride (TMB) and HEPES were from AppliChem (USA). Sulphuric acid and hydrochloric acid were from Reakhim (Russia). Standard PBS tablets (10 mM sodium phosphates + 0.137 M NaCl + 0.0027 M KCl, pH 7.4) were from Ecoservice (Russia). Sodium hydroxide, Na_2-EDTA were from Dia-M (Russia). Lanthanum (III) nitrate, nickel (II) nitrate were from Chemcraft (Russia).

Instrumentation

Multiskan Sky UV-Vis Reader was from Thermo Scientific (USA). ZetaSizer NanoZS particle analyzer was from Malvern (UK). VCX-130 ultrasonic processor was from Sonics & Materials (USA).

Polystyrene ELISA plates with high protein binding were obtained from Kirgen (China).

Buffer for the preparation of LNNP's conjugates: HEPES solution was adjusted to pH 7 with 1 M HCl

Buffers for NLISA:

Coating buffer: 0.2 M sodium carbonate bicarbonate buffer, pH 9.6;

Washing buffer: PBS + 0.1% Tween-20 (PBST).

Substrate buffer: 20 mmol/L of HEPES, 20 mmol/L of MES, 20 mmol/L of sodium acetate, 100 mmol/L of NaCl; pH was adjusted with 5 mol/L NaOH or 5 mol/L HCl.

Substrate solution: 0.55 mL of 4 mg/mL of TMB in DMSO; 9.482 mL of substrate buffer; 0.748 mL of 11.77 M H_2O_2; 0.22 mL of 0.1 mmol/L Na_2-EDTA.

All buffers were prepared using deionized water.

Characterization of $LaNiO_3$@BSA/C6cc.

The size (Z-average, nm) and monodispersity of nanoparticles were measured by dynamic light scattering (DLS). For this, nanoparticles were diluted with deionized water 1:125.

To assess the absorbance at 450 nm of the $LaNiO_3$@BSA/C6cc obtained suspensions were diluted 1:20 in the deionized water+1%BSA+20% glycerol

Concentration of unmodified $LaNiO_3$ nanospheres in suspensions was determined by the gravimetric analysis. One milliliter of suspension was added to the porcelain crucibles and dried to constant weight at +115 °C. Mean of three technical replicates was calculated.

SEM images were obtained using Merlin (Carl Zeiss, Germany) and Hitachi HT7700 Excellence (Hitachi, Japan).

XPS spectra were recorded on X-Ray Photoelectron Spectrometer SPECS (Germany) using Mg K-α excitation (E_{ex}= 1253.64 eV). All spectra were calibrated on C sp2 line (E_b=284.6 eV). XPS data were processed applying the CasaXPS software package. Deconvolution was performed using Shirley type background and Gauss (50%)-Lorents (50%) functions. FWHM for all spectra components for each component of chemical elements (Ni, La) were fixed [1], [2].

X-ray diffraction (XRD) was conducted on a Rigaku Miniflex 600 diffractometer with Co Kα radiation (λ = 1.78897 Å) and the diffraction angle 2θ ranged from 10 to 130° with the step 0.02°. Full-profile fitting of the diffraction pattern was performed using the Rietveld method using FullProf Suite programs. X-ray diffraction (XRD) was conducted on a Rigaku Miniflex 600 diffractometer with Co Kα radiation (λ = 1.78897 Å) and the diffraction angle 2θ ranged from 10 to 130° with the step 0.02°. Full-profile fitting of the diffraction pattern was performed using the Rietveld method using FullProf Suite programs [1].

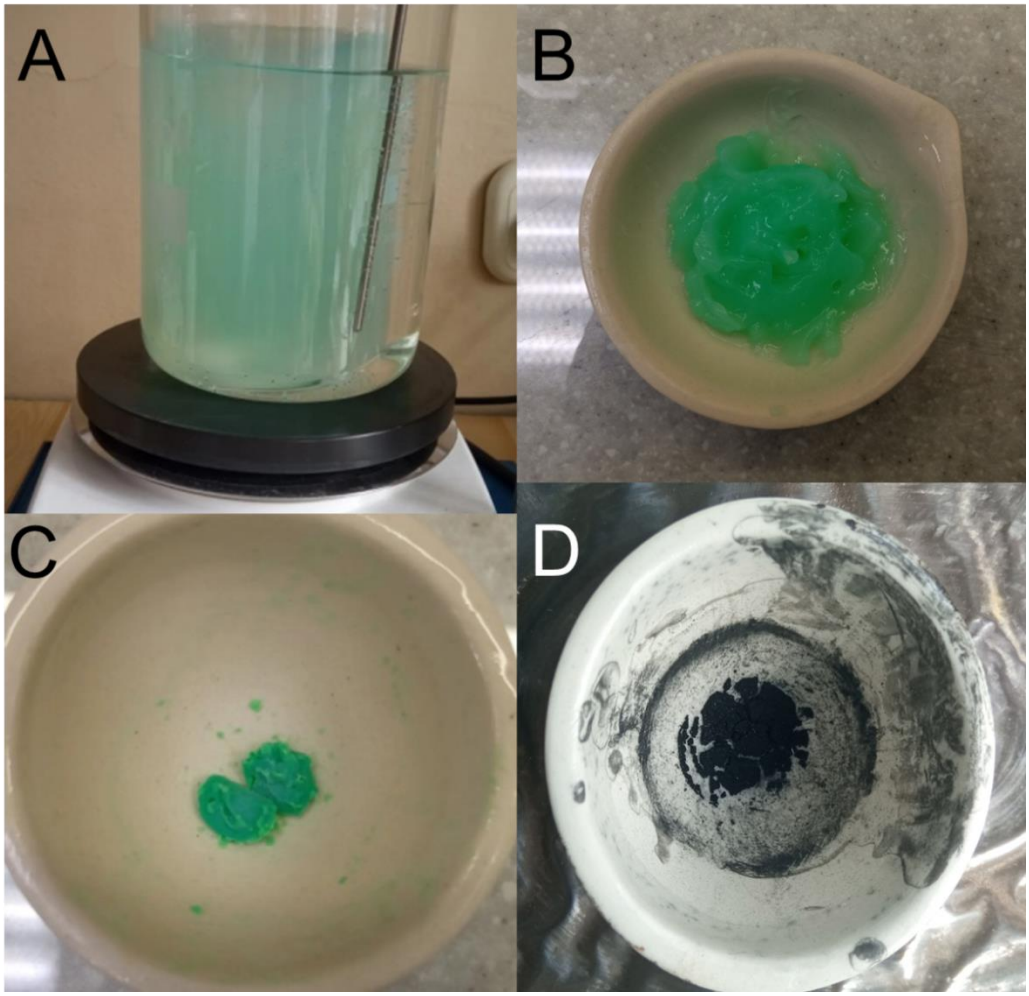

Fig. S1. Stages of synthesis of LNNS. (A) External appearance of LNNS formation upon addition of NaOH; (B) LNNS after precipitation, washing and concentration; (C) LNNS after overnight drying at +37 °C; (D) LNNS after calcination at +650 °C for 2 h.

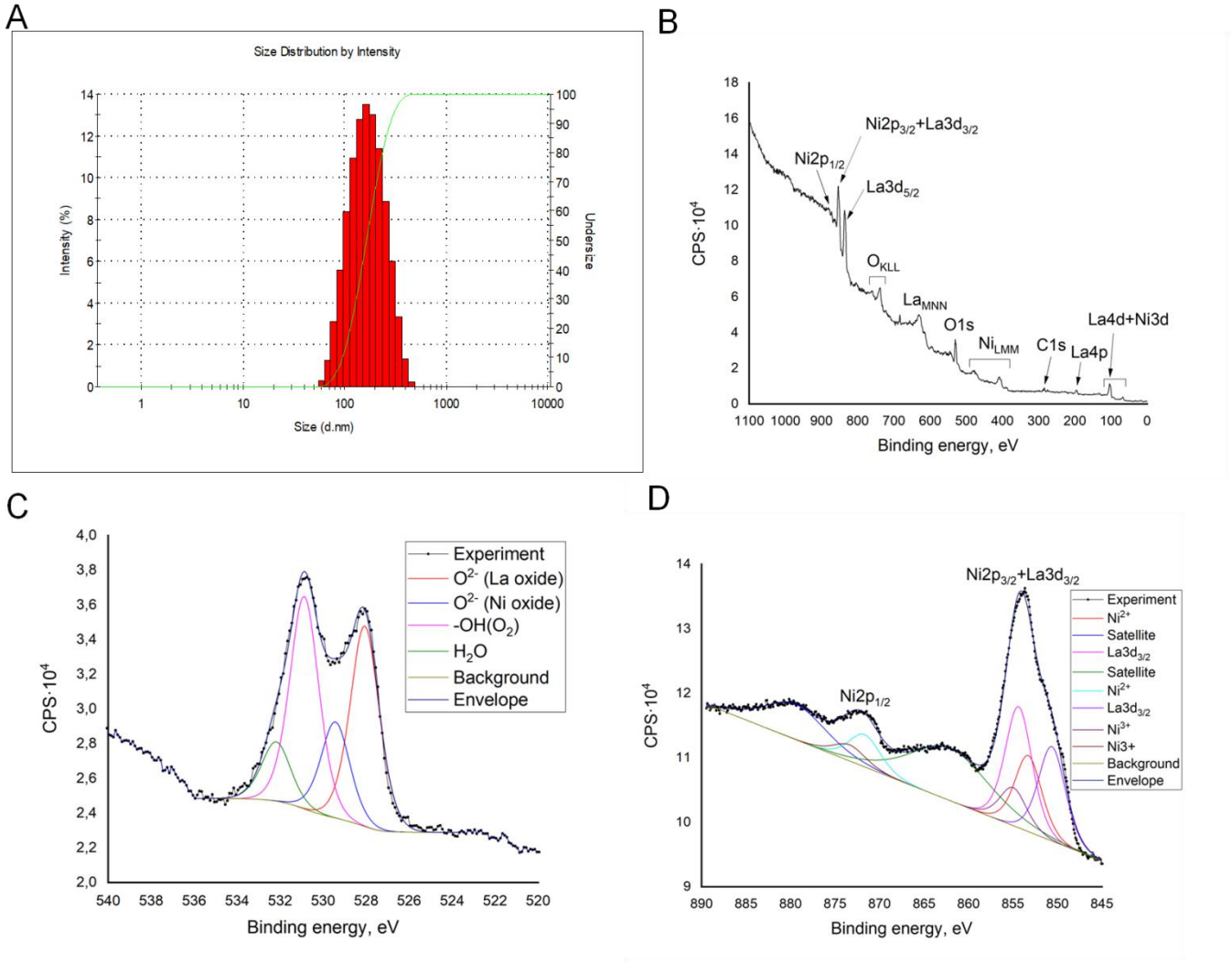

Fig. S2. (A) Size distribution of $LaNiO_3$ NS by intensity. (B) An overview spectra of the $LaNiO_3$ NS sample. (C) XPS signal of $LaNiO_3$ NS sample. (D) Deconvolution analysis of La3d and Ni2p3/2

Figures S3 and S5 show the results of energy dispersive microanalysis. For these studies, suspensions with $LaNiO_3$ (Fig. S3) and $LaNiO_3$@BSA/C6cc (Fig. S4) nanospheres were applied to an aluminum-magnesium alloy substrate and then dried in air. Scanning electron microscopy images were obtained on a Thermo Fisher Scientific Quattro S electron microscope at accelerating voltages in the range of 5 to 10 kV. Energy dispersive microanalysis was performed using an integrated EDAX Octane Elect Plus EDS System spectrometer.

Table S1. Fitting results of La $3d_{3/2}$ and Ni 2p photoelectron spectra of $LaNiO_3$

Bond description	BE, eV	FWHM, eV	Concentration, %
$La3d_{3/2}$	850.15	3.88	11.41
Ni^{2+}	852.98	3.88	13.05
$La3d_{3/2}$	854.29	3.88	22.89
Ni^{3+}	854.68	3.88	6.52
Ni satellite	862.23	8.88	22.89
Ni^{2+}	871.38	4.51	6.52
Ni^{3+}	873.08	3.26	3.26
Satellite	879.12	8.31	13.25

The ratio of Ni^{2+}/Ni^{3+} is about 50%.

Table S2. Fitting results of O1s photoelectron spectra of $LaNiO_3$

Bond description	BE, eV	FWHM, eV	Concentration, %
O^{2-} (La oxide)	528.04	1.61	35.32
O^{2-} (Ni oxide)	529.33	1.61	16.11
-OH (O_2)	530.90	1.61	38.06
H_2O	532.10	1.61	10.50

A

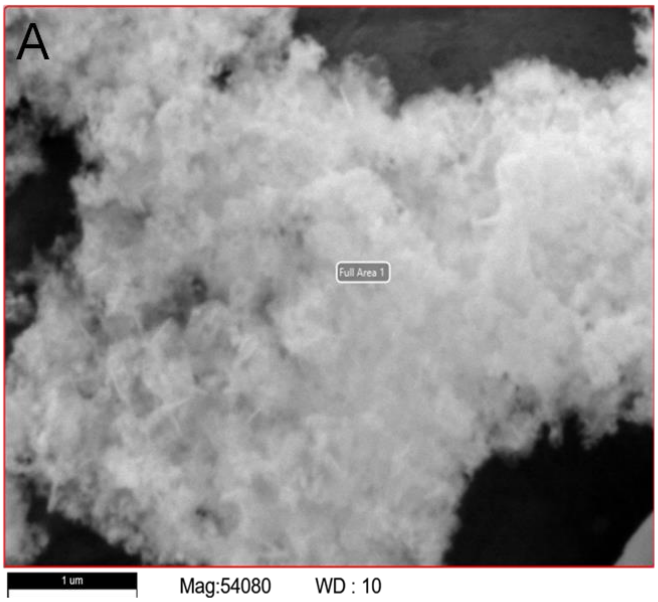

B

Element	Weight %	Atomic %	Error %
C	4.0	9.6	12.3
O	14.7	26.9	7.6
Mg	1.4	1.7	8.6
Al	48.0	52.1	5.0
Ni	10.3	5.1	7.1
La	21.6	4.5	9.8

C

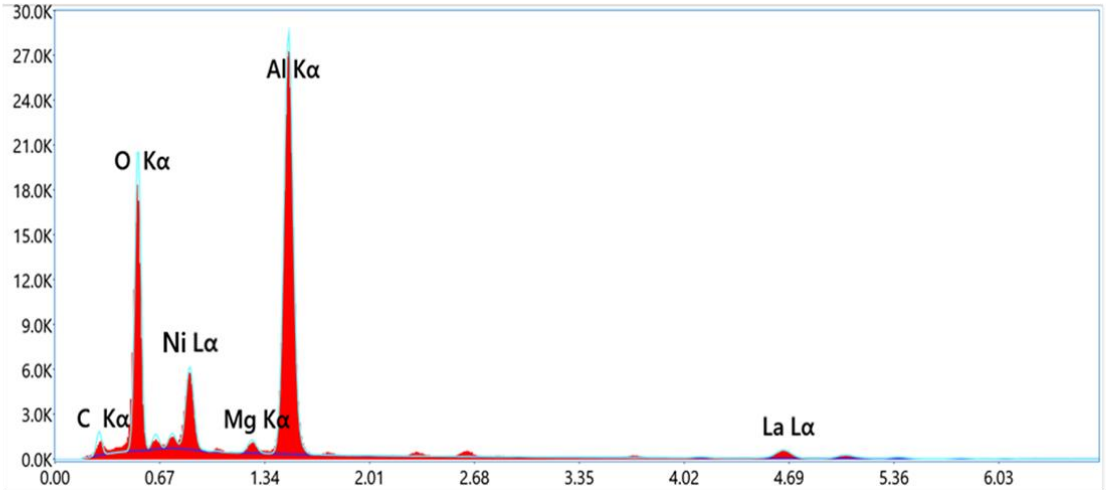

Fig. S3. (A) Signal collection area for the $LaNiO_3$ NS sample. (B) Elemental composition of the $LaNiO_3$ NS sample. (C) Energy dispersive X-ray spectrum for the $LaNiO_3$ NS sample.

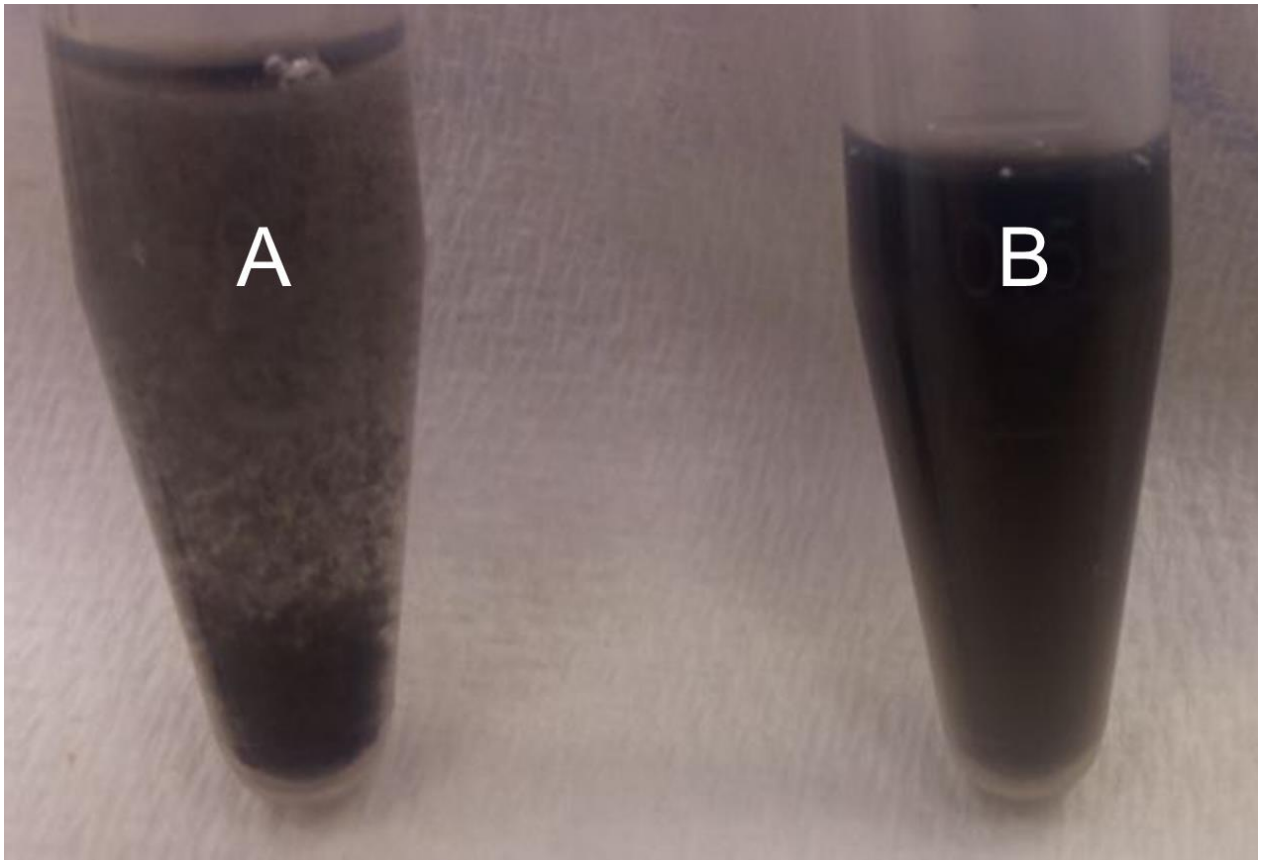

Fig. S4. (A) Aggregation process during fuctionalization stages of the LNNS; (B) Stabilization of the LNNS at the final stage of the diagnostic reagent produce.

A

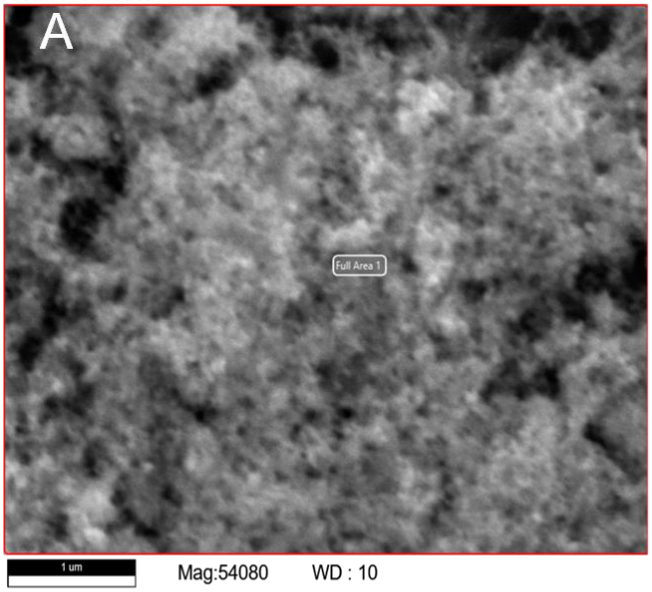

B

Element	Weight %	Atomic %	Error %
C	16.9	30.7	11.1
N	3.6	5.7	10.8
O	9.4	12.9	8.6
Mg	0.8	0.7	7.0
Al	56.8	46.0	3.8
P	2.5	1.7	6.5
Ni	3.5	1.3	7.2
La	6.4	1.0	9.0

C

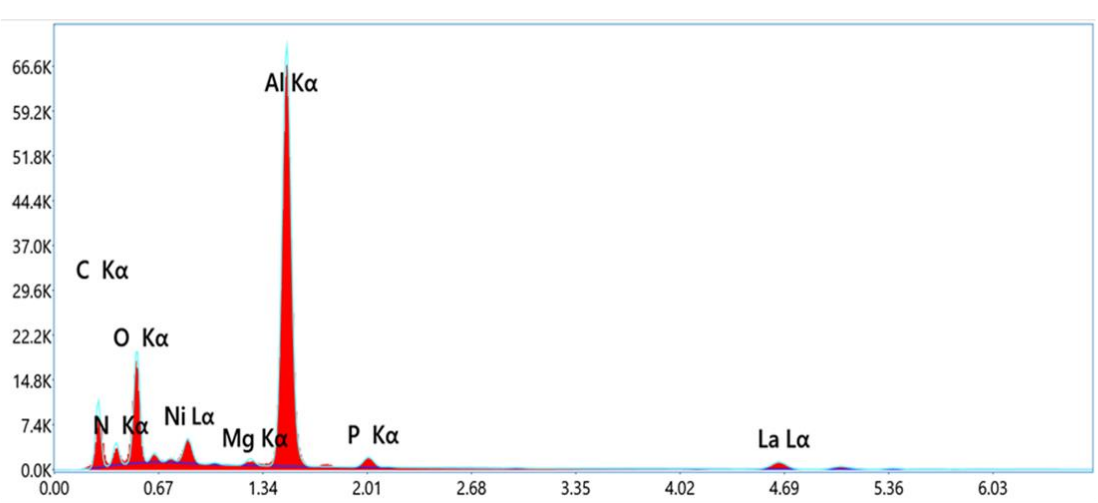

Fig. S5. (A) Signal collection area for the $LaNiO_3$@BSA/C6cc NS sample. (B) Elemental composition of the $LaNiO_3$@BSA/C6cc sample. (C) Energy dispersive X-ray spectrum for the $LaNiO_3$@BSA/C6cc NS sample.

Table S3. Reproducibility of LNNS-based diagnostic reagent synthesis

Serum sample	CRP, mg/L (mean, n=3, Diagnostic reagent #1)	CRP, mg/L (mean, n=3, Diagnostic reagent #2)	CRP, mg/L (mean, n=3, Diagnostic reagent #3)	CRP, mg/L (mean)	Standard deviation	CV,%
1	6.71	5.93	8.19	6.94	0.94	13.49
2	0.29	0.49	0.44	0.41	0.08	20.22
3	5.43	4.94	6.45	5.60	0.63	11.24
4	4.34	4.05	4.30	4.23	0.13	3.12
5	1.46	1.46	1.44	1.45	0.01	0.81
6	0.96	1.01	0.98	0.98	0.02	2.15
7	2.33	2.14	2.05	2.17	0.12	5.36
8	0.86	0.85	0.89	0.87	0.01	1.70

Table S4. Validation of LNNS-based NLISA for CRP detection

Expected concentration, µg/L	Measured concentration, mg/L Mean, n=10	SD (n=10)	CV,%	Recovery index,%
0.098	0.08	0.045	55	62.12
0.195	0.18	0.04	23.5	92.6
0.39	0.42	0.057	13.4	108
0.78	0.81	0.07	8.6	104
1.56	1.595	0.13	8.35	102
3.125	2.67	0.07	2.59	85.36
6.25	6.52	1.05	16.1	104.3
12.5	12.48	1.026	8.22	99.86
25	16.5	2.14	13.32	64.3

Table S5. Spike-recovery test of LNNS-based NLISA for CRP sample in rabbit serum, diluted 1/1000 with blocking solution

Expected concentration, mg/L	Measured concentration, mg/L (n=6)	Recovery,%	SD (n=6)	CV,%
13	13.45	102.9	2.29	13.9
5	3.8	76.2	0.33	8
1	0.8	80.6	0.06	7.66
0.6	0.58	97.3	0.04	6.31
0.35	0.28	78.65	0.025	10.15

Table S6. LNNS-based NLISA precision

Serum sample	CRP, mg/L (mean, n=8)	Standard deviation	CV, %
1	0.6	0.06	11.2
2	12.1	1.821	14.5
3	5.1	0.87	15.4
4	11.1	1.78	16
5	1.4	0.12	8.35
6	1.44	0.18	12.56
7	3.5	0.49	14.05
8	1.3	0.23	17.26

Table S7. LNNS-based NLISA inter-day reproducibility

Serum sample	CRP, mg/L (mean, n=3, day 1)	CRP, mg/L (mean, n=3, day 2)	CRP, mg/L (mean, n=3, day 3)	CRP, mg/L (mean, n=3, day 4)	CRP, mg/L (mean, n=3, day 5)	CRP, mg/L (mean, n=5)	Standard deviation	CV. %
1	1.30	1.36	0.84	0.86	1.16	1.10	0.22	19.60
2	14.82	15.03	12.08	15.40	13.24	14.11	1.26	8.92
3	1.27	1.09	0.75	1.00	0.98	1.02	0.171	16.76
4	12.51	10.90	10.33	9.63	10.23	10.72	0.98	9.16
5	9.34	7.86	8.87	11.31	8.05	9.09	1.24	13.60
6	3.06	2.64	2.60	2.84	2.59	2.75	0.18	6.63
7	16.81	15.76	17.18	15.58	12.98	15.66	1.47	9.40
8	2.37	1.91	1.85	2.03	1.94	2.02	0.18	9.03
9	3.72	4.13	4.09	4.60	4.21	4.15	0.28	6.76
10	3.20	1.95	1.97	2.54	2.15	2.36	0.47	19.88

Table S8. Concentration of CRP in serum samples measured by LNNS-based NLISA and immunofluorescent assay, mg/L

Serum sample	NLISA (n=3)	Immunofluorescent assay (n=3)	Average	% Difference
1	0.35	0.4	0.38	-13.33
2	1.06	1.1	1.08	-3.7
3	17.83	18	17.9	-0.95
4	1.04	1.4	1.22	-29.5
5	0.45	0.5	0.475	-10.53
6	12.5	14.5	13.5	-14.81
7	11.31	12	11.7	-5.92
8	20.04	19.9	19.97	0.7
9	105.73	104.9	105.3	0.79
10	130.88	117.4	124.1	10.86
11	5.41	6.1	5.76	-11.99
12	3.2	2.5	2.85	24.56

References

[1] P. Li, C. Tian, W. Yang, W. Zhao, Z. Lü, LaNiO3 modified with Ag nanoparticles as an efficient bifunctional electrocatalyst for rechargeable zinc–air batteries, Front. Mater. Sci. 13 (2019) 277–287. https://doi.org/10.1007/s11706-019-0474-z.

[2] Y. Qiu, R. Gao, W. Yang, L. Huang, Q. Mao, J. Yang, L. Sun, Z. Hu, X. Liu, Understanding the Enhancement Mechanism of A-Site-Deficient $La_x NiO_3$ as an Oxygen Redox Catalyst, Chem. Mater. 32 (2020) 1864–1875. https://doi.org/10.1021/acs.chemmater.9b04287.